DIFFUSION OF GASES AND LIQUIDS IN NANOPOROUS SOLIDS

By

MOUMITA BISWAS

Bachelor of Technology in Chemical Engineering

West Bengal University of Technology

Kolkata, West Bengal

2016

Submitted to the Faculty of the
Graduate College of the
Oklahoma State University
in partial fulfillment of
the requirements for
the Degree of
MASTER OF SCIENCE
May, 2023

DIFFUSION OF GASES AND LIQUIDS IN

NANOPOROUS SOLIDS

Thesis Approved:

Dr. Jeffery L. White

Thesis Adviser

Dr. Clint P. Aichele

Dr. Seokjhin Kim

Dr. Jimmie Weaver

ACKNOWLEDGEMENTS

Many people have contributed to this thesis either directly or indirectly. I thank my advisor Dr. Jeffery L. White, my advisory committee members, Dr. Clint P. Aichele, Dr. Seokjhin Kim and Dr. Jimmie Weaver, and the School of Chemical Engineering for their continuous support and guidance during my graduate years at Oklahoma State University. I acknowledge my mentors and lab mates, Anya Zornes, Omio Rani Das, Sarah Horstmeier, and Amir Erfani Khaneghahi, for mentoring me in my research and assisting me in completing my thesis work. All errors that are contained in this thesis are, however, attributable only to me.

Most of all I thank my family and friends, for their patience, encouragement and support in life and also in pursuing this academic degree.

Name: MOUMITA BISWAS

Date of Degree: MAY, 2022

Title of Study: DIFFUSION OF GASES AND LIQUIDS IN NANOPOROUS SOLIDS

Major Field: CHEMICAL ENGINEERING

Abstract: The diffusion of gases and liquids under nanoconfinement is of fundamental importance for understanding various processes like catalysis, enhanced oil recovery, and CO_2 sequestration. The present contribution narrates how diffusion NMR was used as a quantitative method to study the transport of probe molecules in nanoporous solids when the fluids are subjected to variable pressure. Nanoporous glass (NPG) and zeolites have been considered for investigation in this work. NPG was selected as a model system to study confinement effects, diffusion, and partitioning of liquid water and liquid cyclohexane. Self-diffusion coefficients of methane were measured in several commercially-important zeolites as a function of pressure, with a specific focus on experimental reproducibility and minimization of error in the calculated diffusivities. To identify differences in transport properties on modification of zeolites with different silica to alumina ratios, methods such as ammonium-hexa-fluoro-silicate (AHFS) treatment, phosphoric acid treatment, steaming, and, lanthanum ion exchange were employed. Variable pressure of nitrogen gas and methane were applied to the NPG and zeolites samples, respectively and their self-diffusion coefficients were measured. One of the primary outcomes of the research was the development of a complete method for introducing gases into nanoporous solids, specifically zeolite catalysts, at variable pressure that yields highly reproducible diffusion coefficients. With these improvements, the NMR diffusometry experiments have revealed that CH_4 at elevated pressure is a sensitive probe of both chemical and topological perturbations to zeolite catalyst structures, and thereby applicable to a variety of systems in which sorbents, reagents, and surfactants are sequestered in nanoporous hosts.

TABLE OF CONTENTS

Chapter Page

I. INTRODUCTION 1

Overview 1
Intellectual Merit 2
Broader Impact 2

II. REVIEW OF LITERATURE 3

Importance of zeolites in hydrocarbon diffusion 3
Diffusion-limited reaction 5
Fundamentals of diffusion 8
NMR diffusometry 13
Intraparticle vs interparticle diffusion 18
Hypothesis 19

III. METHODOLOGY 20

Materials 20
Sample preparation 20
Vacuum drying process 20
Gas pressure in NMR tube 22
Steaming method via water bubbler 25
Steaming method via autoclave 26
NMR 27

Chapter Page

IV. RESULTS AND DISCUSSIONS....28

NPG control experiments....28
Zeolite experiments....31

V. CONCLUSIONS AND FUTURE DIRECTIONS....46

REFERENCES....49

APPENDICES....61

LIST OF TABLES

Table Page

1. Pressure (atm), diffusivity coefficient (m^2/s) and standard deviation for pure methane gas. The diffusion time is 10 ms. 35
2. Pressure (atm), diffusivity coefficient (m^2/s) and standard deviation for methane gas in NH4-ZSM-5 Si/Al= 15 & Si/Al = 40. The diffusion time is 10 ms. 37
3. Diffusivity coefficient (m^2/s) and standard deviation for methane gas in H-ZSM-5 Si/Al= 15 & Si/Al = 40. The diffusion time is 10 ms. 37
4. Diffusivity coefficient (m^2/s), $<R^2>$ (m^2) and root mean square displacement R (m) for methane gas in a variety of ZSM-5. The diffusion time is 10 ms. 42
5. Diffusivity coefficient (m^2/s) and standard deviation for methane gas in H-ZSM-5 Si/Al = 15 and PZSM-5 Si/Al = 15 (P/Al = 1:1). The diffusion time is 10 ms. 43
6. Diffusivity coefficient (m^2/s), $<R^2>$ (m^2) and root mean square displacement R (m) for methane gas in HY, LaY 1X1C and LaY 2X2C. The diffusion time is 10 ms. 44

LIST OF FIGURES

Figure Page

1. Molecules migrating through the zeolite channels. Reproduced from reference 10 with permission. 1
2. a. Tetrahedral arrangement of the SiO_4 and AlO_4 molecules forming unit blocks of a zeolite. b. 2D representation of framework structure of zeolite. Reproduced from reference 20. 4
3. a. Different regimes of diffusion b. Plots for diffusion coefficient vs. pore diameter and activation energy vs. pore diameter. Reproduced from reference 34. 5
4. Spin-echo diffusion NMR spectra with decaying signal intensities as a function of gradient strength. Reproduced from reference 83 with permission. 13
5. Schematic depicting effective sample volume for diffusion NMR experiments. The zeolites with gas molecules diffusing through the channels. 14
6. Sequences that represent the steps in which radio frequency (RF) produces to NMR signal. a) The spin echo (SE) sequence b) The stimulated echo (STE) sequence. 15
7. Schematic diagram for vacuum line showing the vacuum drying process of zeolite. 22
8. Schematic diagram of pressure manifold used to introduce variable-pressure gas into nanoporous solid hosts, including zeolite catalysts. 23
9. Schematic diagram for steaming of zeolite using water bubbler method. 25
10. Schematic diagram depicting vapor flow from liquid in flask to NPG in NMR tube using vacuum line. 26
11. Reduced diffusivities (D_{app}/D_0) of water and cyclohexane in (a) oil rich (90% v/v oil 10% v/v water), (b) water rich (10% v/v oil 90% v/v water) mixtures confined at different pore fillings in 10-nm NPG and (c) water and cyclohexane (measured separately) in confinement at different pore fillings inside 10-nm NPG. D_{app} is the apparent self-diffusion coefficient and D_0 is self-diffusion coefficient for the free fluid ($D_\circ$ for water and cyclohexane measured separately). The effective gradient pulse duration (t_g)=1 ms and diffusion time (Δ) = 50 ms. Reproduced from reference 119 with permission. 29
12. Effect of pore filling on chemical shift for the water-rich mixture (10/90 v/v% C6H6/H2O) confined in 10 nm nanoporous glass. a) Pore filling = 27.5%. b) Pore filling = 47.5% c) Pore filling = 85%. The C6H6/H2O peak area integrals for the 27.5, 47.5 and 85% loadings were 0.07, 0.11, 0.07 respectively. The spectra are plotted according to the intensity of the largest peak, not total area. Reproduced from reference 119 with permission. 30
13. Diffusivities of a. cyclohexane and b. water separately in 10-nm NPG. The diffusivities are measured at three different controlled pressure of 1bar, 4 bar, and 8 bar of nitrogen gas. 32
14. ^1H single-pulse NMR spectrum of CH_4 gas in H-ZSM-5 at 120 psi pressure. 33

Figure Page

15. a. Plot for Diffusivities (m^2/s) vs. Pressure (atm) of pure methane gas. The diffusion time is 10 ms. The error bars are plotted as one standard deviation. b. Diffusivity (m^2/s) vs. diffusion time Δ (ms) for pure methane, methane in HY and its La modified counterparts LaY 1X1C and LaY 2X2C.....36
16. a. Plot for Diffusivities (m^2/s) vs. Pressure (atm) for NH4-ZSM-5 Si/Al= 15 & Si/Al = 40 and b. Diffusivities (m^2/s) of methane with standard error bars in H-ZSM-5 with Si/Al of 15 and 40. The diffusion time is 10 ms. The error bars are plotted as one standard deviation. 38
17. Plots of signal intensity vs. gradient strength square (G^2/m^2) for a variety of a. HZSM-5 Si/Al = 15 and b. AHFS washed ZSM-5 Si/Al = 15. The diffusion time is 10 ms. 39
18. Plot of signal intensity vs. gradient strength square (G^2/m^2) for a variety of ZSM-5 catalysts as indicated. The diffusion time is 10 ms. 40
19. Diffusivities (m^2/s) of methane with standard error bars in H-ZSM-5 and P-ZSM-5 (P/Al = 1:1) with Si/Al = 15. The diffusion time is 10 ms. The error bars are plotted as one standard deviation. 43
20. a. Diffusivities (m^2/s) of methane with standard error bars in HY and LaY 1X1C. b. Diffusivities of methane in HY, LaY 1X1C and LaY 2X2C. The diffusion time is 10 ms. The error bars are plotted as one standard deviation. ..45

CHAPTER I

INTRODUCTION

Overview: Diffusion is a transport phenomenon that occurs in all states of matter. It has the potential to reveal answers to some of the fundamental questions related to physical, biological, and chemical processes that are yet unknown. More specifically, studying diffusion can answer questions on molecular interactions at microscopic level in catalysts.[1,2] Important experimental and theoretical developments on how diffusion occurs in various materials have been established to study such systems.[2,3]

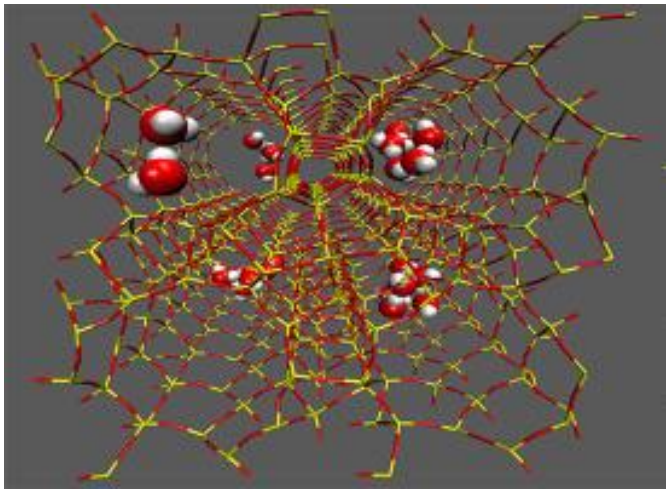

Figure 1. Molecules migrating through the zeolite channels. Reproduced from reference 10 with permission.

Over the last few decades, interest has increasingly grown towards understanding the molecular behavior of liquids and gases within complex porous geometries and in confinement on molecular length scales, i.e., nano-confinemnent.[1,3,4] The foundation of the subject relies heavily on the classical theories of diffusion.[3,5] With the advent of new technologies, the curiosity to explore into the sciences of the intricate materials have peaked.[1,2,4] Zeolites are microporous structures that are widely used for heterogeneous catalysis.[2,6] In general, it has been the focus of research to

describe how hydrocarbons specifically interact with zeolites of different compositions by measuring diffusion directly using nuclear magnetic resonance (NMR).[7,8] NMR techniques allow investigation into different time scales as well as length scales at which molecules interact, thus providing a comprehensive understanding of the processes.[8–10] Figure 1 shows the diffusion of molecules through the cage-like zeolite channels.

Intellectual Merit: The importance of the diffusion and interaction of hydrocarbons in nanoporous media, especially zeolites is ever-growing.[3,4] With the following research work, we seek to contribute to the literature on mobility of probe molecules in nanoconfinement. Different chemical modifications have been applied to zeolites in order to understand the changes that occur in interactions between the sorbed molecules and the surface of zeolites. The aim of the study is to identify the trends that emerge from diffusivity coefficients of gases in zeolite and understand the behavior of individual liquids and their mixtures under confinement of nanoporous glass (NPGs).[11,12] These trends may provide insight into the diffusion of gases and liquids in nanoporous hosts, and have implications for future technical applications.

Broader Impact: Zeolites and NPGs have a variety of applications. Zeolites are highly efficient catalysts, adsorbents and ion exchangers, and are used throughout the petroleum and chemical industries.[3,6,13] Zeolites' effectiveness in these applications has lead the scientific community to investigate their applicability in the fields of renewable energy and other environmentally important areas, such as, energy storage, carbon dioxide sequestration, air pollution remediation, etc. The ability of zeolites to act as molecular sieves opens up tremendous possibilities for zeolites to be employed in numerous areas of technology. While NPGs can be used as model systems to study subsurface phenomena of fluids. The studies conducted on diffusion of probe molecules in nanoporous media of zeolites and NPGs will impact all the diverse domains, such as petrochemical, agriculture, water treatment etc., that they find application.[13–17]

CHAPTER II

REVIEW OF LITERATURE

Importance of zeolites in hydrocarbon diffusion: Zeolites have gained special attention in the research community from both practical and theoretical perspectives, due to their applicability in adsorption, separation, and catalysis.[14] Synthetic zeolites are efficient in various large scale operations such as hydrocarbon conversion, gas separation, ion exchange and catalytic processes, due to their reactivity and high shape-selectivity.[14,18–20] Zeolites are microporous, crystalline aluminosilicates that have intra-framework porous channels and/or cages. The conventional zeolite structure consists of three-dimensional networks of TO_4 (T = Si, Al) tetrahedral, most commonly $[SiO_4]^{4-}$ or $[AlO_4]^{5-}$ linked with O atoms connecting neighboring tetrahedral. Other than the intra-framework aluminum, extra-framework aluminum (EFAL) species are present in the zeolite structure in cationic $Al(OH)^{2+}$, $Al(OH)_2^{+}$, AlO^{+} and other forms.[21,22] The composition may contain up to three components, that is, extraframework cations, framework aluminosilicates and the sorbed phase water molecules and hence, the following is taken as the general formula for zeolites:

$$M_{x/n}\,(AlO_2)_x(SiO_2)_y \cdot\ zH_2O \qquad \ldots(1)$$

with M as the compensating cation of the negatively charged framework, y/x is the Si/Al ratio, and z is the number of molecules of water attached.[18,23] Figure 2 displays the tetrahedra arrangement of the SiO_4 and AlO_4 molecules to form unit block and represent the framework structure of zeolites.

The Si/Al ratio of zeolites is of enormous importance as it can vary over a wide range and impart ratio specific property, majorly hydrophilicity. Zeolites with high Si/Al ratio, known as high-silica zeolite, have high hydrophobicity due to the nonpolar nature of the Si-O-Si surface.[24] Thermal treatments and other modifications enable tampering with Si/Al ratio. Zeolites are classified into various categories based on pore size of the channels. Pore sizes of zeolite has a range of 0.2 to 0.8 nm. Small pore size zeolites have 0.20–0.45 nm diameter, medium pore size comprises of 0.45–0.60 nm and large pore size comprises of 0.60–0.80 nm. In this research work, the 0.54 nm medium pore size zeolite of ten-membered rings, that is ZSM-5 and 0.74 nm large pore size of 12-membered ring, that is, zeolite Y have been considered for experiments.[3,13,19,23,25] Bronsted and Lewis acid sites contribute to the acidity of zeolite which facilitates hydrocarbon transformation reactions. Brønsted acid sites (BAS) act as proton donors and are present as Bridging [Si-OH-Al] hydroxyls whereas the 4-coordinate Al associated with

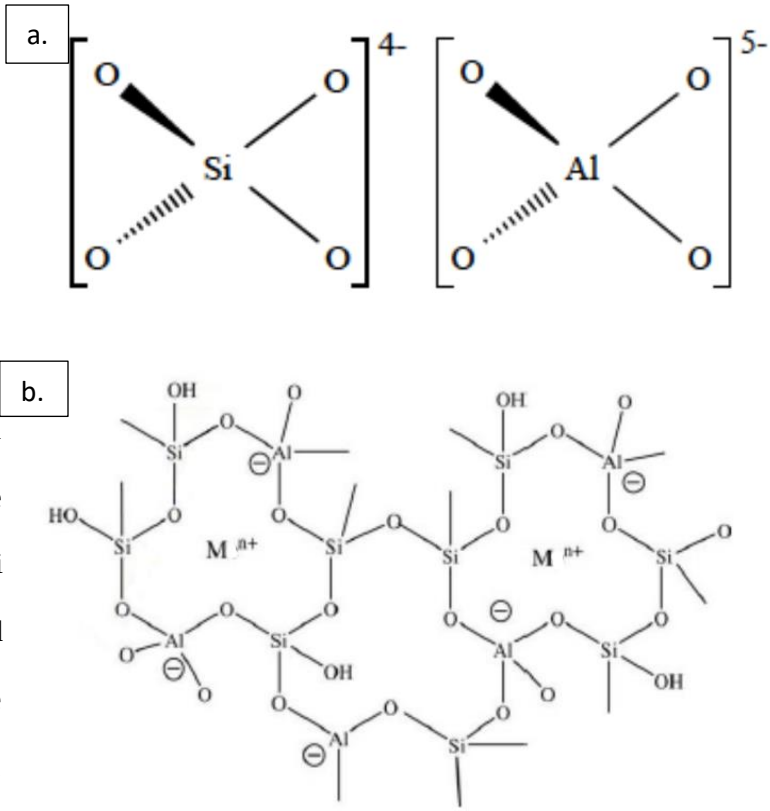

Figure 2. a. Tetrahedral arrangement of the SiO_4 and AlO_4 molecules forming unit blocks of a zeolite. b. 2D representation of framework structure of zeolite. Reproduced from reference 20.

BAS can be partially released from the framework by dealumination treatment, leading to the formation of EFAl species within the pores of zeolites. These EFAL species are often referred to as Lewis acid sites (LAS).[26,27] Catalytic activity, transport of key intermediates and interaction between hydrocarbons and the zeolite surface are essential components of product selectivity in heterogeneous catalysis. Hence, understanding the diffusion of hydrocarbon is crucial in order to develop, design and optimize the very process of catalysis.[23,28–31] Diffusion in zeolites is an activated process, that is, the activation energy for diffusion is primarily responsible for the different diffusivities of various components.[25,32]

Diffusion-limited reaction: Another major aspect to note here is that the shape-selectivity of molecules in zeolite is driven by diffusion. They are important separating agents of hydrocarbon mixtures as it is an interplay of the three main regimes of diffusion: molecular, Knudsen and intracrystalline diffusion. The different regimes of diffusion are shown in figure 3a. Figure 3b shows the plots of diffusion coefficient and activation energy vs. pore diameter. Intracrystalline diffusion regime has the lowest diffusion coefficient and highest activation energy. Certain reactions that occur on the surface of catalyst depend solely on the rate at which the sorbate particles diffuse to the site of reaction, such reactions are termed as the

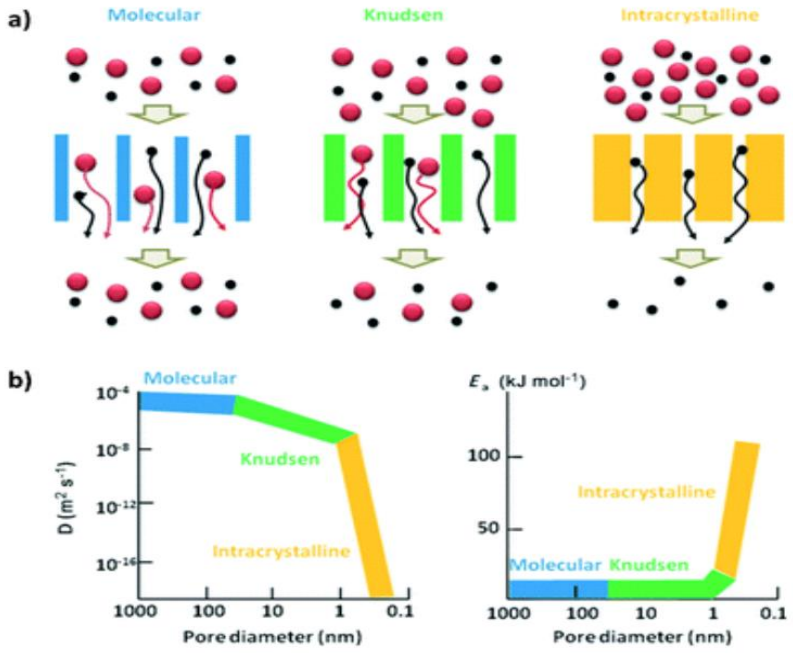

Figure 3. a. Different regimes of diffusion b. Plots for diffusion coefficient vs. pore diameter and activation energy vs. pore diameter. Reproduced from reference 34.

diffusion-limited reactions. In the micropores of a zeolite, the activated diffusion regime governs the process due to the pore size being comparable to the size of diffusing molecules.

Activated/intracrystalline/configurational diffusion, also referred to as restricted diffusion, occurs when molecular sizes of diffusing fluids are appreciably larger than the pore opening resulting in hindrance of the fluid's entry into such pores.[33,34] The low rate of migration within the micropores cause a slow rate of reaction at the active sites. The Thiele modulus η and the effectiveness factor φ are indicators of diffusion limitations and are related by the equation given below:[29,35–37]

$$\eta \equiv \frac{measured\ activity}{activity\ without\ diffusion\ limitation}, \quad \varphi \equiv \sqrt{\frac{intrinsic\ rate}{diffusion\ coefficient}};$$

$$\varphi = \sqrt{\frac{R^2 k C^{n-1}}{D}}$$

$$\eta = \frac{3}{\varphi}\left(\frac{1}{\tan(\varphi)} - \frac{1}{\varphi}\right)$$

…(2)

In these equations, R is the particle size, k is the intrinsic reaction rate constant, C is the reactant concentration inside the particle.[29,38]

A large Thiele modulus reflects a low rate of diffusion, which means the reaction is diffusion-limited.[29,38] Methanol-to-hydrocarbon (MTH) reactions on SAPO-34 zeolite that has large CHA cage of 0.94 nm in diameter and a small eight-ring pore 0.38 nm opening,[39,40] $(CH_3)_2O$ conversion with H-ZSM-5[41,42] and C_3H_6 cracking with zeolite Y[43] are some diffusion-limited reactions in which the reaction rate is entirely dependent on the rate at which solute molecules diffuse. SAPO-34 catalysts generally encounter transport limitations that causes coke deposition, and this is one of the common drawbacks of diffusion-limited reactions.[44] As another example, in xylene isomerization and C_7H_8 disproportionation reactions on ZSM-5, the large difference in

diffusivity of the products causes effective trapping of undesired isomers, thus, enhancing selectivity of a specific isomer.[45,46] Voogd and coworkers have demonstrated that the difference in diffusivities caused shape selectivity of 3-methylpentane and n-hexane reactants, thus facilitating the process of cracking on H-ZSM-5.[47] Analyzing the activation energies of those reactions using Arrhenius plots provided insight on intracrystalline diffusion-limitation of both 3-methylpentane and n-hexane cracking rates at high temperatures within the catalyst. The plots indicate that there is a decrease in the activation energy over heterogeneous catalysts of similar physical and chemical nature.[47] Further details on Arrhenius plots have been discussed in later sections of this literature review.

It has been observed that the varied applications can be targeted by manipulating the size, shape, and interconnected channels of zeolites through the synthesis methods. Often extreme restraints are imposed on selectivity of products due to confinement effects and diffusion limitations. So, posterior introduction of porosity at meso- and macroscales bestows a solution to such deterrents, and this has, in turn, unfolded multiple perspectives that are being discussed in the literature currently. These ideas related to 'hierarchical' zeolite have facilitated enhancement of adsorption, molecular sieving ability and catalytic performances as they exhibit refined molecular diffusion characteristics.[48–51] Guenneau's group has demonstrated experimentally that interconnectivity exists between the mesoporous and microporous channels.[52] The mesopores provide new paths, creating access to the interior of the zeolite. Hence, a pathway to the microporous space is generated as an alternative to the existing intraframework channels, that leads to faster diffusion of the particles.[52] In certain cases, it has been noted that mesopore generation within zeolites either does not tamper with Bronsted acidity or can act beneficial through Lewis-Bronsted-synergism.[53] However in other cases, such as, the introduction of mesopores in HZSM-5 by one-step desilication and reassembly, there was a decrease in Bronsted acid sites, increase in medium acid sites and formation of diverging pore structure leading to enhanced catalytic

stability.[54] Bonilla et al. shared a unique remark on the hierarchical SAPO-34, that although these materials have the capability to enhance the mass transfer in microporous domain, the magnitude of that improvement is dependent to a large extent on the connectivity and availability of the pores and channels. They further suggested that, while the reduction of surface barriers leads to such improvements, the effective diffusivity can be significantly increased only if the microporous volume fraction is below the percolation threshold, which means that the connected transport pores would not exist above the volume fraction of micropores.[55]

Fundamentals of diffusion: As mentioned previously, diffusion in zeolites has been the focus of discussion and research interest of the scientific community over several decades now. It is an interdisciplinary subject that has gradually incorporated diversified methodologies. The theoretical foundation of the subject combined with practical experimental methods originate from the classical theories of diffusion in different states of matter. There is a tendency of any type of matter, solid, liquid or gas to migrate from one position to another to reach a state of equilibrium, thus, eliminating any variation in the concentration and uniformity is attained. The time scale at which this migration takes place is tremendously varied. For gases, it could be less than a second whereas for solids, it can take up to decades for some cases. Therefore, time scale is a major factor to determine the significance of diffusion on an empirical basis.[3–7] In this research work, we try to explore the relevance of the transport of fluids in the field of catalysis, oil and gas, energy storage, etc. Therefore, it is important to understand different aspects of diffusion and transport processes. We have investigated how fluids diffuse and interact with nanoporous solids such as nanoporous glass (NPG). Diffusion, being a property of matter, is projected by its tendency towards maximum entropy and the mechanism generally depends on the nature of diffusing particles and their interaction with their surroundings.

The activation energy of diffusion plays a key role in the diffusion process.[19,56–58] Gas-kinetic models have been developed to evaluate the diffusion coefficients that form the backbone

of measuring the translation motion of the particles. The coefficient of diffusion is expressed by combining the mean velocity and mean free path, along with other factors, such as, temperature contributing to the transportation process. These migrating particles have a mean free path that is the simplest derivation of an expression for the distance travelled by them between two successive collisions. For pragmatic purposes, the frame of reference and the time scale at which the diffusion experiment is being considered becomes significantly relevant. Diffusion can be broadly classified into two different phenomena that is the mass transfer or transport diffusion which takes place due to concentration gradient and the other being Brownian molecular motion or self-diffusion which is followed by tracing the trajectory of the molecules and determining the mean square displacement of the path.[3,59–61]

The challenge of accurately predicting transport properties is a major concern and Einstein obtained a relation to examine the model of a solution. The typical relation that was aimed to resolve the issue is known as Stokes-Einstein equation:

$$D = RT/6N\pi\eta r \quad \ldots(3)$$

where R is the ideal gas constant, N is the Avogadro's number, T is the absolute temperature, η is dynamic viscosity, and r is the radius of the diffusing particles.[62–64]

It is a significant hydrodynamic law that combines the Einstein relation and Stokes law to relate the self-diffusion coefficient D to the shear viscosity for dense fluid. Einstein had shown that the relation between the movement of molecules and diffusion coefficient can be expressed with the following equation:

$$< R^2 > = 6Dt \quad \ldots(4)$$

where R is the radius, and t is the time.[65–68]

Another key aspect of diffusion is to understand its driving force. The process of diffusion is driven by concentration gradient of the solute molecules and that is formulated by Fick's first law.

$$J = -D\frac{\partial C}{\partial x} \quad \ldots(5)$$

in which J is the flux ($cm^{-2}s^2$), $\frac{\partial C}{\partial x}$ is the negative gradient of concentration (cm^{-4}).[69,70]

Since diffusion exhibits the tendency to attain equilibrium at a macroscopic level, the gradient of chemical potential can be accounted as the force that drives diffusion.

$$J = -\frac{RT}{f}\frac{d\ln p}{d\ln c}\frac{dc}{dz} \quad \ldots(6)$$

with $\frac{d\ln p}{d\ln c}$ representing the gradient of the equilibrium isotherm in logarithmic coordinates, and f is simply representing a friction coefficient.[3]

Fickian diffusion is easy to analyze as it's driven by the penetrant concentration gradient and does not create a stress field in fluids unlike non-Fickian diffusion in which diffusion occurs without obeying the Fick's law. Non-Fickian diffusion is primarily observed in some polymer systems that have sharp boundary separating a highly swollen region from a dry, glassy portion and the stress related to viscoelastic behavior of the system results in a negative convex flux. For non-Fickian diffusion in a polymer-solvent system, the diffusion coefficient at constant temperature is dependent on solvent concentration and time and the diffusing penetrant causes a deformation that produces a stress which then interacts with the Brownian motion of the fluid molecules. This type of transport is increasingly being used in applications such as gas separation, protective clothing, drug delivery, etc. The degree of swelling in the material has a direct consequence on its kinetics and performance. The transport of solvent molecules through polymeric materials is complicated

in nature depending on several factors, such as temperature, chemical properties of diffusing molecules, the physical characteristics of the polymer, their interaction with each other, and any external mechanical deformation. Materials like conductive polymer poly(pyrrole), phosphorous, etc. exhibit non-Fickian characteristics.[71–73]

One of the mechanisms that determines the rate of transport of particles if the mean free path of the molecule lambda is comparable or larger than the pore diameter d of the medium, is termed as Knudsen diffusion, which is predominant in materials with pore sizes between 2 to 50 nm. This leads to collisions between the particles and the pore wall being more frequent than interparticle collisions.[29,74] Thus, the molecular trajectories become mutually independent and can be evaluated in terms of a set of chords of the pore network. Also, as λ is dependent on the pressure P and temperature T through the kinetic theory relationship λ proportional to T/p, it is observable in macroscopic systems at quite low pressure or high temperature. However, it plays a crucial role in the transportation of gas molecules in the restricted geometries. The random nature of this mechanism is equivalent to the Fickian expression for flux in which the diffusivity is dependent only on the pore size and the mean molecular velocity.[75,76] In the Knudsen regime, the diffusion is strongly dependent on the interfacial geometry and the connectivity of pore network whereas weakly dependent on temperature and independent of pressure because the interparticle collisions are not accounted for in the mechanism.[77] Knudsen number is used to measure the importance of Knudsen diffusion in a system, and it must be greater than one to indicate that the system is dominant in Knudsen regime.[78] Questions have been raised on whether microporous zeolites have Knudsen regime prevalent in the migration of guest molecules. This doubt appears due to the heavy influence of van der Waal forces on the molecules that enter the channel of 0.4-0.7 nm diameters but there is no quantitative evidence for the magnitude of reduction in diffusivity.[79]

Particles in the lower-pressure system diffuse faster than those in the higher-pressure systems as they interact with more particles and come under the influence of their force fields. In a

macroscopic sense, diffusion is a time dependent process, and the rate of mass transfer is known as diffusion flux.

$$J = \frac{1}{A}\frac{dM}{dt}$$

...(7)

where A denotes the area across which diffusion is occurring, M is the number of atoms diffusing through and t is the elapsed diffusion time.

If the diffusion flux is independent of time, a steady state condition exists. In steady state diffusion, the concentration of species at each surface, when they are diffusing from a region of higher concentration (pressure) to a region of lower concentration over a distance, is held constant. The concentration gradient is given by:

$$\text{concentration gradient} = \mathrm{dC/dx}$$

…(8)

The constant of proportionality D is combined with the negative concentration gradient to get the Fick's first law equation mentioned previously. Usually practical diffusion are non-steady-state ones in which the diffusion flux and the concentration gradient at any point vary with time. Eventually, this develop into Fick's second law:[80,81]

$$\frac{\partial C}{\partial t} = D\frac{\partial^2 C}{\partial x^2}$$

…(9)

NMR diffusometry: The translational motion that emerges from the migration of particles from one spatial location to another due to thermal energy or chemical potential of the system, is termed as self-diffusion and this can be characterize quantitatively to get the self-diffusivity coefficient. It plays a central role in transport at the molecular level and thus, governs the kinetics to a great extent.

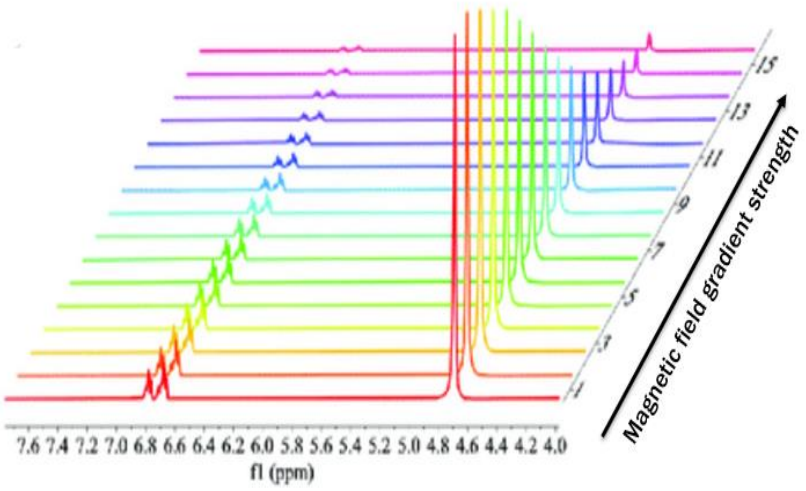

Figure 4. Spin-echo diffusion NMR spectra with decaying signal intensities as a function of gradient strength. Reproduced from reference 83 with permission.

Considering the difficulties to measure the translational motion without having any detrimental effects on the outcome, nuclear magnetic resonance (NMR) is one of the most powerful tools that provides a means of non-invasive measurements of self-diffusion. NMR diffusometry is used in a way acquire information about the structures, motions, reactions, and interactions of the molecules without significantly perturbing them. Importantly, magnetic moments are very sensitive to their surroundings and yet interact with them without much disturbance. NMR utilizes the magnetic field gradient methods to investigate the molecular migration in zeolitic adsorbate and adsorbent system by encoding the physical position of the particle.[82–84] It has been intensively used to analyze the structure of porous geometries, such as porosity, pore size distribution, permeability, water saturation, and a variety of processes that occurs in them. To determine the fundamental dynamics of diffusion of the particles present in the sample, it needs to be put into the spectrometer while being mindful that the system conventionally captures the signal once the radio frequency is applied and echo attenuation takes place.[85–87] The mechanism is governed by the principles of interaction of magnetic dipole or electric quadrupole moments of the nuclei of the molecules with their

neighbors. Pulsed field gradient (PFG) NMR technique is considered one of the most reliable methods to determine self-diffusivity. The PFG technique determines mean square displacement for a particular time interval and is given by:

$$z_{rms} = \sqrt{2Dt} \quad \ldots(10)$$

where, z_{rms} represents the time average root mean square distance travelled by a group of molecules within an effective sample volume. Therefore, the self-diffusivity coefficient has a unit of m^2/s.[88–92]

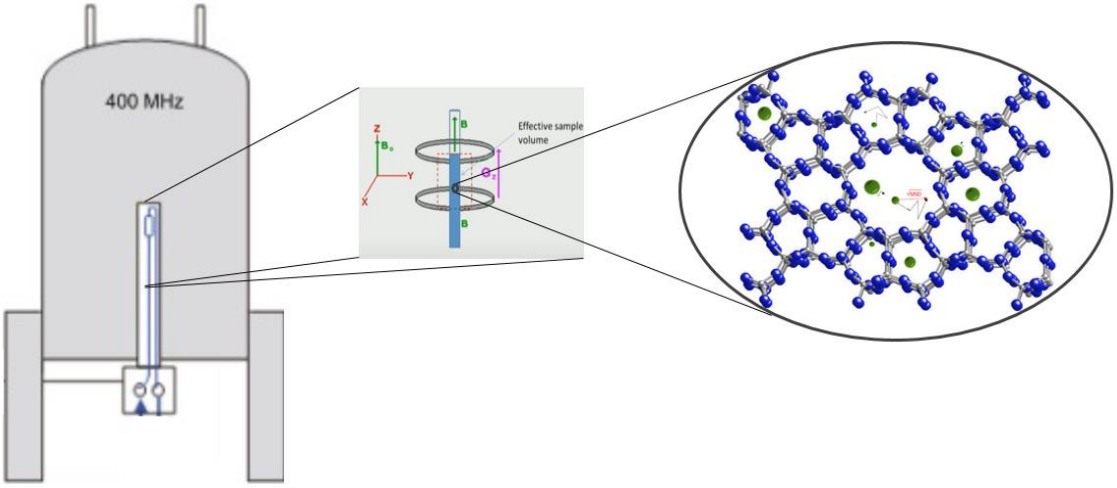

Figure 5. Schematic depicting effective sample volume for diffusion NMR experiments. The zeolites with gas molecules diffusing through the channels.[2]

Hahn discovered the spin-echo phenomenon and soon after it was realized that it has the potential to measure the translational motion of particles.[93] Without the presence of gradient pulses, the detected signal gets attenuated only by transverse relaxation during the 2τ period. Thereafter, the steady gradient spin echo (SGSE) NMR diffusion measurements was developed within the next decade, but it had certain limitations associated with it. To overcome the challenges, Stejskal and Tanner introduced the application of magnetic gradients as pulses in the spin-echo sequence in 1965 that is known as pulsed gradient spin-echo (PGSE) NMR technique today. On application of

pulsed field gradients, refocusing of signal occurs based on the time interval between the pulses and attenuation of the detected signal is dependent on the displacement of the particles during the delay period delta. Due to relaxation losses and coupling evolution during transverse relaxation, the spin-echo is no longer the most used diffusion measurement method as it leads to undesirable signal distortion. These challenges can be overcome with the application of stimulated-echo (STE) sequence.[8,94–96] Figure 6 shows the steps involved in the spin-echo and stimulated-echo sequences. The difference occurs due to the splitting of π into two π/2 pulses that increases the diffusion delay time by the spacing. Since, the attenuation of the echo occurs from increasing observation times that arises primarily from longitudinal (T1) rather than transverse (T2) relaxation, this procedure leads to a much less steep decay of signal intensity with observation time. Thus, it increases the magnetization time for stimulated echo sequence.[2,3]

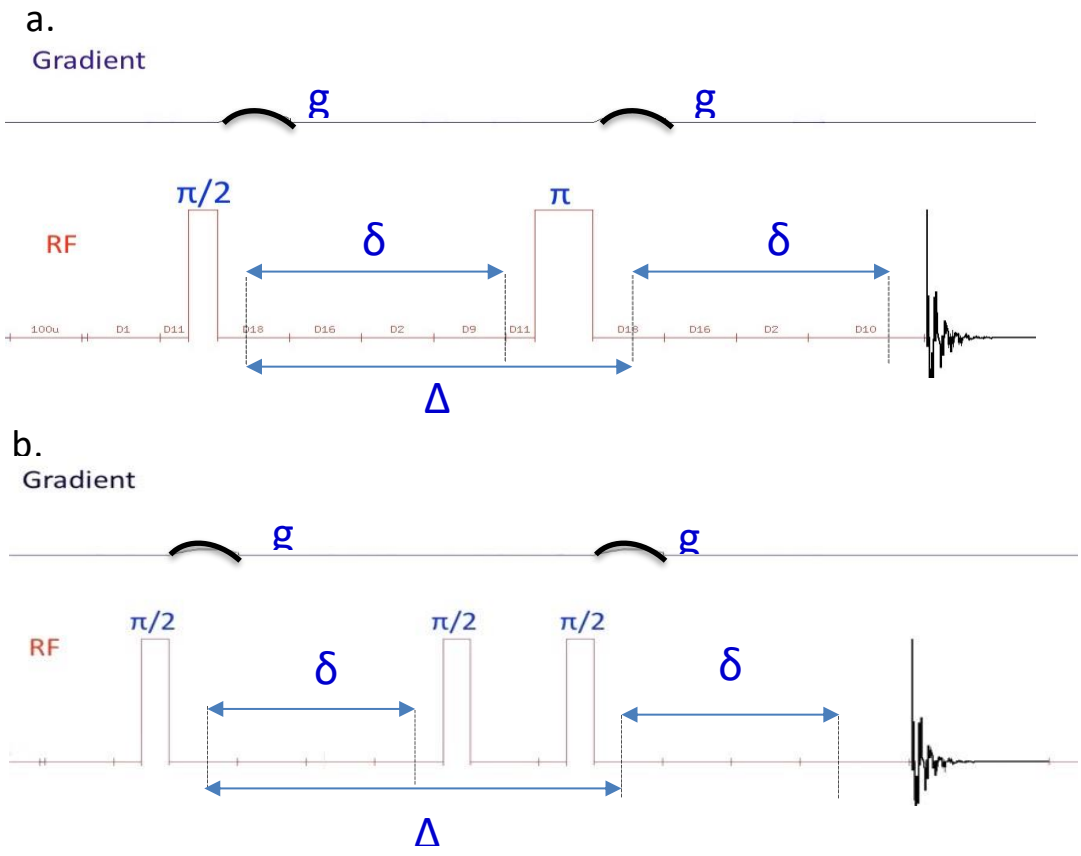

Figure 6. Sequences that represent the steps in which radio frequency (RF) produces to NMR signal. a) The spin echo (SE) sequence b) The stimulated echo (STE) sequence.[3]

Stejskal and Tanner derived a theoretical expression of the effect of a time-dependent magnetic field gradient and verified it experimentally as well. The equation is given below:

$$I = I_0 \exp\left[-D\gamma^2\delta^2 g^2\left(\Delta - \frac{\delta}{3}\right)\right] \quad \ldots(11)$$

In the above equation, I is the intensity of the signal, Io is the intensity of signal without echo attenuation, D is the translational diffusion coefficient of the molecule, γ is the gyromagnetic ratio of the nuclei, δ is the pulse field gradient duration, Δ is the diffusion delay time, and the g is the gradient strength.[94,96–98]

Woessner was the first to note the effects of confined diffusion in SGSE experiments with sample of benzene in rubber.[99] Among the various techniques of NMR, Karger and Ruthven have considered PFG NMR to be the most effective method. They demonstrated the application of NMR diffusometry to analyze elementary diffusion processes in microporous solids, specifically zeolites. According to them, the stimulated echo is method that overcomes the challenges posed by the primary echo technique which is related to the improvement of observation time due to the time dependence of spin echo amplitude on transverse NMR relaxation. They have discussed about the sorption kinetics of microporous catalysts that have been observed to be usually influenced and even dominated by diffusion in the extracrystalline pores that are classified as mesopores and macropores. Further, their analysis presented that there is consistency in the correlation between the diffusional activation energy for a small pore adsorbent to the size of diffusing hydrocarbon molecules. This in turn portrays that the diffusion process in the small pore zeolites is controlled by the energy barrier prevalent in the passage through the windows of zeolite.[3,100–104] Therefore, NMR diffusometry acts as a tool to determine the self-diffusivity coefficients and activation energies of hydrocarbons in zeolites using the diffusion coefficient-Arrhenius relationship:

$$D = D_o exp\left(-\frac{E}{RT}\right)$$

…(12)

Here, D_o is the constant independent with temperature, E is the activation energy for diffusion, T is the temperature and R is the gas constant with the value R = 8.31 J/(K mol).[105,106]

Some research works are dedicated to meticulously understanding the relation between diffusion and activation energy of various materials. Hong et al. studied diffusion anisotropy with methane in HZSM-5 crystals at sorbate concentration of 12 molecules per unit cell. They determined the activation energies to get Arrhenius plot which showed that the ratio of diffusivities in the plane xy to z direction is of the order 4.5.[107] Grenier et al. developed a new i.r. method to measure the sorption rate in zeolite crystals by tracing the transient temperature response on the surface of the crystal. Limiting activation energy data from NMR diffusometry experiments and zero-length column value concur well with the results from the new method.[108] Price and co-workers conducted experiments to examine the translational motion and activation energy of supercool water molecules by applying PGSE NMR method. They found the diffusion of supercooled water has a smooth declining trend and its behavior change to non-Arrhenius as the temperature decreased to 238 K.[109] Another set of research work by Price and coworkers on diffusion measurements of Lysozyme aggregation show that monomeric lysozyme does not vary its aggregation state with temperature as the self-diffusion coefficients abide to an Arrhenius relationship.[110] Chmelik's group demonstrated that the combination of PFG NMR and magic-angle spinning helps in observation of ethene/ethane molecules in both gas and adsorbed state. Their team determined the activation energy for diffusion of ethane in ZIF-8 crystals is comparatively higher than that of ethene through evaluation of diffusion selectivity of the both the types of hydrocarbons.[111] Stallmach's group has performed NMR experiments to measure diffusivity coefficients of C3-C4 n-alkanes and alkenes in CuBTC. This led them to find out that the activation energies of alkenes increase by about 7 kJ/mol compared to same number of carbon atom

alkanes.[112] Kimmich and Bachus investigated and discussed the observations on temperature dependence of self-diffusion coefficients of molten form of polyethylene and polystyrene through modified NMR method.[113] They concluded that other than the random direction factor n-1, there are three more sources to the molecular weight dependence of self-diffusivity coefficient in polymer melts and they are the intrinsic molecular weight dependence of curvilinear reptation diffusion, molecular weight dependence of free volume and lateral displacements. These accumulation of research works show the connection between activation energy and diffusivity and how they assist in tapping into the various applicability of migration of molecules to contribute to existing literature base.[113]

Intraparticle vs interparticle diffusion: As mentioned previously, zeolite encounters both intraparticle as well as interparticle diffusion. Due to the presence of both types of diffusion, it opens the opportunity for the research community of explore the variations that can be produced by tailoring the zeolite structure. The intraparticle diffusion occurs within the porous structure and it is a slow process with lower diffusivity due to increased wall effect and some steric hindrance. It is the domain in which the molecules are found in adsorbed state and could be attached to a carrier molecule for migration purposes. When interparticle diffusion takes place within zeolites, the probe molecules move alone with less constraints and thus, diffusivity is increased to quite an extent. It has been reported that NMR signal results from the superimposition of the signals arising from both intraparticle and interparticle diffusion. Since the mobility of the in these two domains are usually different the respective diffusivities may be found by resolving the echo attenuation into two different components in accordance with the equation below:

$$\varphi(\Delta) = exp\left[-\gamma^2\delta^2 g^2\left(D_2 + \frac{p_1 D_1}{\gamma^2\delta^2 g^2 \tau_2 p_1 D_1 + 1}\right)\Delta\right] \quad \ldots(13)$$

with g as the field gradient, γ is the duration of pulse, δ denotes gyromagnetic ratio, p_1 and p_2 denote the relative number of molecules in the inter and intra regions, respectively. Also, D_1 and D_2 are the diffusivities in the inter and intra regions, respectively and Δ is the observation time.[3,7]

Hypothesis: Taking into consideration all the aspects discussed above, *we hypothesize that diffusion NMR is a quantitative method to understand diffusion of liquids and gases in nanoconfinement when the fluids are subjected to variable pressure and it can be used to identify differences in transport properties arising from altering the chemistry, silica to alumina ratio and post-synthetic modifications of the nanoporous hosts*. Recent report by Van Speybroeck et al. suggests promotional effect of presence of Bronsted acid sites on the diffusivity of alkenes in SAPO-34 zeolites. They conducted experiments to acquire details relating to diffusion of paraffins and olefins in the intracrystalline space of 20-30 mm large zeolite crystals. PFG-NMR technique was used to measure self-diffusivity of ethane and ethane in H-SAPO-34 and the results indicate a favorable effect of increasing the number of Bronsted acid sites on diffusivity of ethene whereas, for ethane in H-SAPO-34, no such correlation was found.[114] Another report by Vasenkov et al. demonstrates optimization of molecular sieving in zeolitic imidazolate framework (ZIF). They designed samples and put multiple loading pressure of hydrocarbon to perform the diffusion NMR experiments.[115,116] Similarly, we aim to synthesize samples of different type of zeolite and tailor them to observe their effects on the self-diffusivity of hydrocarbons. The hydrocarbons could be alkane or aromatic that are suitable to move through the micropores of the zeolite. The pressure loadings of the hydrocarbons are a major component to determining the variation in their kinetic behavior as they migrate through the porous channels of the zeolite.

CHAPTER III

EXPERIMENTAL METHODOLOGY

Materials: The primary materials were zeolites with different Si/Al ratios, phosphoric acid (H_3PO_4), lanthanum nitrate ($La(NO_3)_3$), ammonium-hexa-fluoro-silicate (AHFS), methane (CH_4), sodium hydroxide (NaOH), water (H_2O), nanoporous glass (NPG), nitrogen gas (N_2), cyclohexane (C_6H_{12}), deionized water.

Sample preparation: The first step to prepare a zeolite sample for NMR experiments is to convert it to proton form at high temperature because the commercial zeolite that is available in the market is found usually in the ammonium or sodium cation form. The vacuum setup that is established in our laboratory is used to convert the ammonium or sodium form of zeolite to its proton form. NH_4^+- exchanged zeolite ZSM-5 (Si/Al = 11.5; Si/Al = 15, CBV 302E; Si/Al = 25; Si/Al = 40 CBV 8014; Si/Al = 140) and zeolite Y samples were obtained from the supplier Zeolyst.

Vacuum drying and calcining process: Appropriate amount of the zeolite was weighed and put to heating in glass vessels under vacuum condition. The weight was measured to be 150±10 mg as it is the optimum amount that can be converted to proton form in our laboratory glassware with minimum to no ammonium cation presence and that has been verified through solid-state NMR experiments. A clean glassware/vessel, that was not contaminated with any other type of zeolite powder, was taken and the measured zeolite was poured into it. The zeolite powder

forms a bed with large radius and surface area exposed at the bottom of the glassware that has large cross-section area. The glassware was attached to its top component that had valve on it with grease and then, connected with the vacuum line with an O-ring and a clamp. The pressure within the glassware is dropped very slowly stepwise, so that the powdered zeolite is not sucked into the vacuum due to large pressure drop. After multiple small release of air from the glassware to the vacuum line, the pressure has dropped to a large extent. When the release of air did not cause much fluctuation in the manometer display values, the vessel was completely opened to the vacuum line. The minimum value the manometer connected of vacuum pump showed was $3.6x10^{-2}$ mbar.

Next, as figure 7 shows, the heater was placed around the glassware in a way that the zeolite is present at the middle of the height of the heater as shown in the figure and then, it was turned on. The temperature of the vessel was raised to 500˚C to convert the zeolite, usually ZSM-5 or zseolite Y, from NH_4^+ form to proton form, that is, H-ZSM-5 and HY. The heater is connected to a temperature controller (Omega, CN616A series). The ramp and soak feature of the temperature controller was used for elevating the temperature in a stepwise manner to ensure minimal damage to the zeolite structure. The temperature was ramped up to 100˚C at a rate of 0.5˚C/min, soaked at 100˚C for 2 hours to remove the moisture first, then ramped up to 500˚C at 0.5˚C/min and finally, it was held at 500˚C for 12 hours and later, stepwise cooled down. The valve of the glassware was closed to seal it from the atmosphere before detaching it from the channel of the vacuum line that was also closed through a valve. The sealed glassware with calcined sample was put into in a glovebox filled with argon. The glassware was opened and the argon gas was allowed to flow into it. The top section of the glassware was removed and the grease was cleaned. The proton form of the sample was transferred into an NMR tube. Then, tube was sealed with controlled atmosphere valve (New Era NE-CAV5) to avoid contact of sample with moisture once it was taken out from

the glovebox. The sample was ready for getting pressurized with hydrocarbon through the manifold.

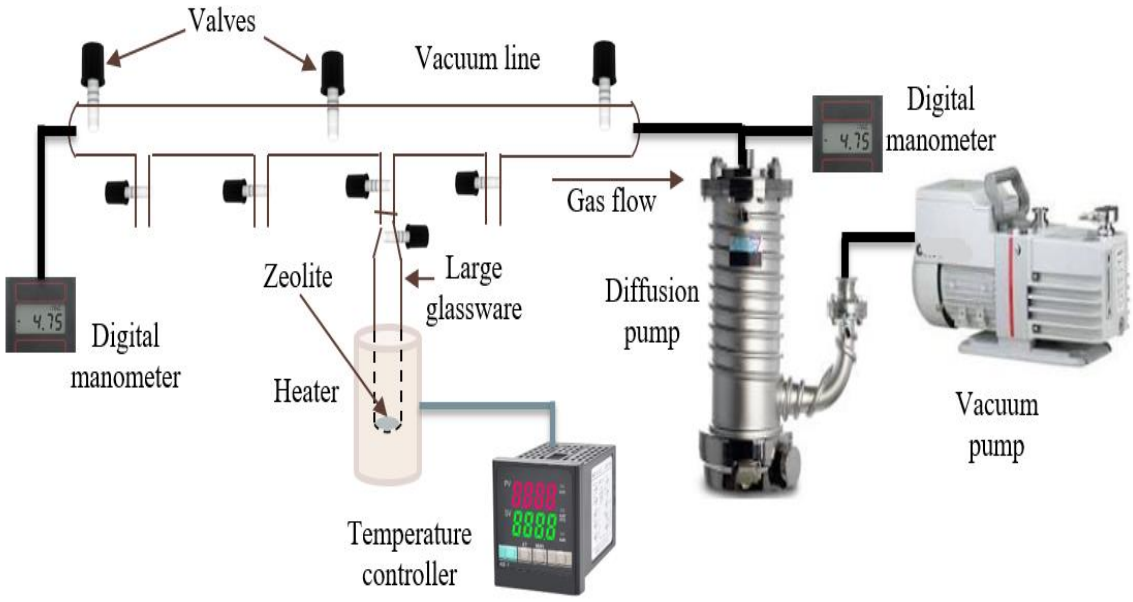

Figure 7. Schematic diagram for vacuum line showing the vacuum drying process of zeolite.

Gas pressure in NMR tube: Subsequently, the sealed NMR tube, that either contains argon or has been vacuum sealed, was connected to the pressure manifold as shown the figure 8. The valves on the pressure manifold is closed and checked thoroughly for safety purposes. The valve on the gas cylinder was opened and the pressure gauge connected to the mouth of the cylinder was adjusted according to the requirements. On opening the right-most valve on the manifold, the gas flowed through the line and the pressure gauge on the manifold measure the magnitude of the pressure. Next, the sealed NMR tube was attached to the manifold using an adapter. Once the NMR tube and the manifold interlocking was tight and secure, the gas was allowed to flow into the middle section of the manifold where the control valve was attached. The central two-way valve was closed and the left-most valve was opened. Then, the control valve was opened released the pressure of the gas mixed with air. This step was repeated 2-3 times to eliminate the air present in the manifold that can supply moisture to the calcined sample. Before allowing the full pressure on the NMR

tube, the controlled atmospheric valve (CAV) at the top of NMR tube was opened. The valves on the manifold were closed and opened alternatively to let the argon gas from the NMR tube be release through the control valve. This step was repeated twice to eliminate the possible presence of argon gas. All the two- way valves were opened and the gas was flowing throughout the manifold. The NMR tube was pressurized with hydrocarbon, such as, methane. The pressure gauge connected to the manifold that was right above the attached NMR tube measured the pressure in it. On getting the pressure to the desired level, the CAV was sealed back to the tube and the pressure above it was released for it to be safely detached from the manifold. Thereafter, the pressurized sample in the NMR tube was sonicated for 30 min to facilitate the uniform distribution of the zeolite powder. This procedure made the sample ready for NMR diffusometry experiments and it can be placed into the coil of the gradient probe.

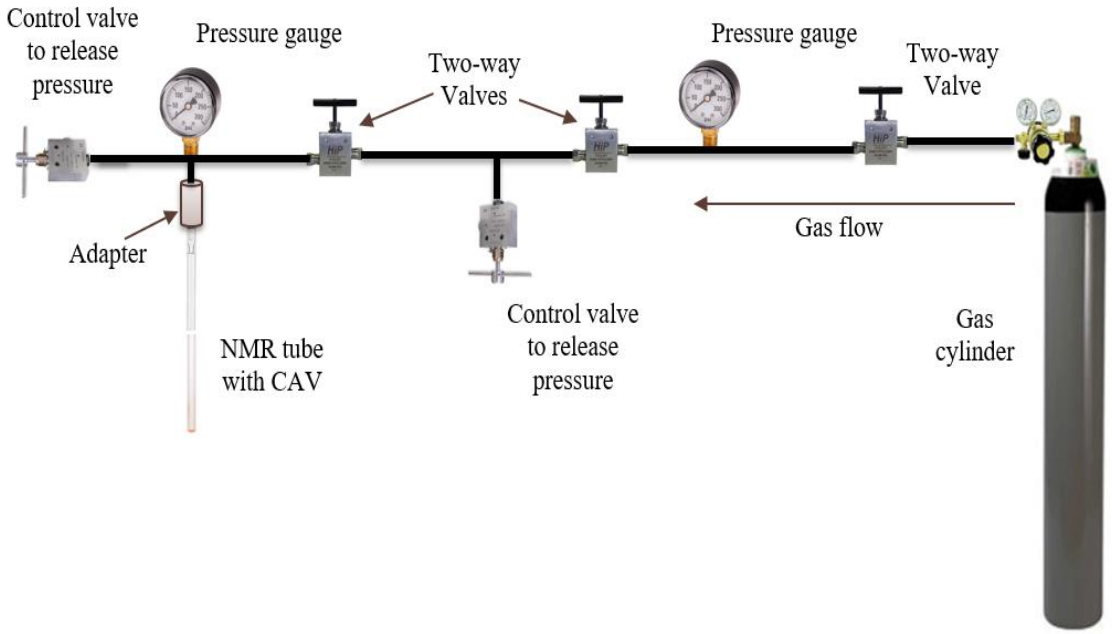

Figure 8. Schematic diagram of pressure manifold used to introduce variable-pressure gas into nanoporous solid hosts, including zeolite catalysts.

For AHFS washing of zeolites, NH_4^+-form of zeolite was weighed in a balance and put in water to create a zeolite solution. The solution was heated and stirred for 10 minutes. In the meantime, AHFS solution was prepared using weighed AFHS and water. It was stirred and added to a burette. As the zeolite solution was being stirred and heated, the AHFS solution was added to it dropwise from the burette. Few drops of 1M NaOH was added to the resultant solution to bring the pH up to 5. The temperature of the closed lid beaker that contained the resultant solution was maintained at 90˚C for 4 hours. Later, the solution was filtered using hot deionized water and the solid residue was put in oven to dry for 8 hours at 80˚C. After that the dried residue is crushed to turn it into powder and put to vacuum drying. Once vacuum dried, the same procedure is followed as mentioned above, that is, it is put in NMR tube and pressurized with hydrocarbon for diffusion NMR experiments.

To synthesize LaY, cation exchange procedure was considered. The H^+ form of zeolite Y was obtained from vacuum drying it at 500˚C. It was then treated with 0.1M aqueous $La(NO_3)_3$ at 90˚C under stirring condition for 6 hours. The resulting solution was centrifuged. As the reside separated from the supernatant, the later was discarded. The exchange cycle was repeated thrice to remove exchangeable protons. The solid residue after the last cycle was added to deionized water and stirred for 6 hours at 90˚C. Later it was washed thrice with deionized water at room temperature and this method was repeated twice. So, after numerous washes at 90˚C and at room temperature, there was a complete removal of excess physiosorbed cations from the catalyst. The catalyst was dried and made ready for NMR diffusometry. Similarly, to prepare P-ZSM-5, the NH_4^+-ZSM-5 was converted to H-ZSM-5 through calcining at 550˚C. Later, H_3PO_4 was added via incipient wetness to produce modified P-HZSM-5 and it was vacuum dried at 500˚C. If the exchange process and vacuum drying were performed once on the sample it's referred to as LaY 1X1C and when it's performed twice it's referred as LaY 2X2C in the later sections.

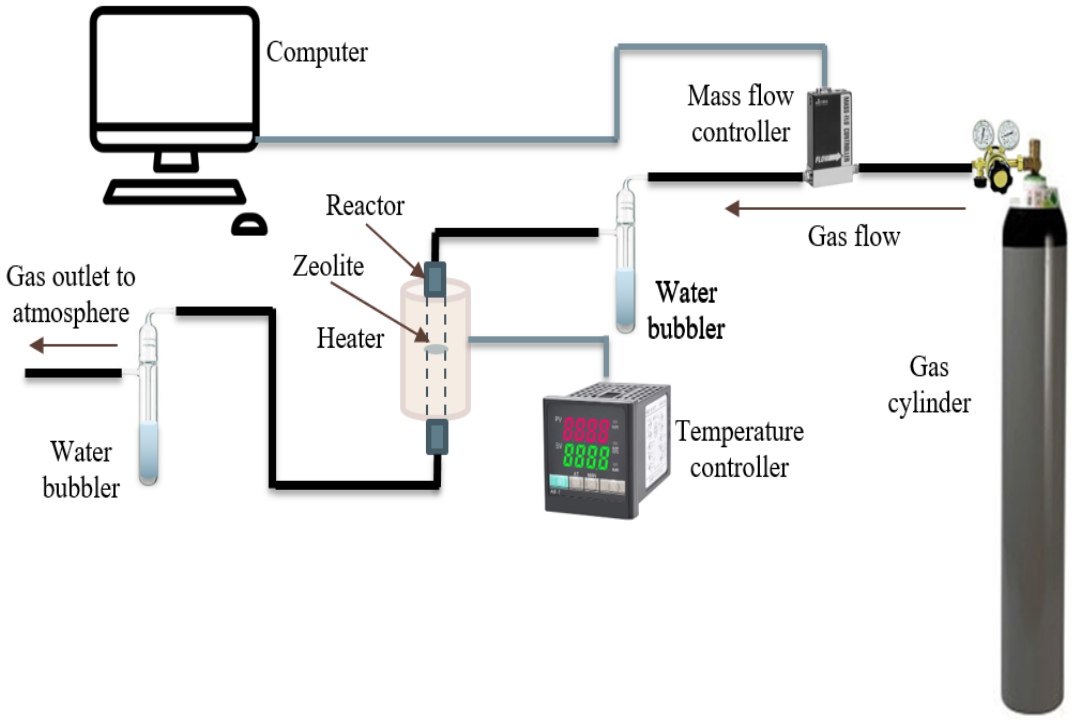

Figure 9. Schematic diagram for steaming of zeolite using water bubbler method.

Steaming method via water bubbler: Steaming is performed for stabilizing the zeolite structure. There are various methods associated with steaming and we have considered two of them in this work, this is, the water bubbler and autoclave methods. The stabilization process during steaming leads to Al atoms to get expelled from the zeolite lattice and form nonframework Al species.[117] Calcined samples were weighed to 80-90 mg and put in a nest of glass-wool. Then, it was transferred to a micro-reactor that was place within a heater. The heater was connected to a temperature controller with ramp and soak feature. The zeolite was treated by steaming with 21 Torr water vapor in an air flow at 15 mL/min in a flow reactor with water bubbler, heated stepwise to a final temperature of 600°C, and held there for 72 h. After steaming, the samples were dehydrated using the flow reactor with nitrogen gas at 500°C for 5 h. Figure 9 shows the schematic diagram for the steaming of zeolite with various components connected to complete the system.

Steaming method via autoclave: Using another method of steaming,[118] selected sample of dry zeolite was placed in an autoclave, suspended in a beaker. Water was placed at the bottom of the autoclave, not directly in contact with the zeolite. Then, the 100-ml autoclave was heated up to 200°C to generate steam at the autogenic pressure for 24 hours. The vapor pressure of water at this temperature is 18.6 atm. Under these conditions, the gas compressibility factor for water is about 0.96. Therefore, 50 mmoles (n_0) of water will be required to reach the saturation of the vapor at this temperature in the 100 ml volume. We use the n/n_0 ratio to represent the amount of liquid water placed in the autoclave for each experiment plus the amount of water already present inside the zeolite relative to the number of moles at saturation (n_0). That is, one would not expect liquid water on a flat surface when $n/n_0 < 1$. After 24 hours of steaming, the zeolite was taken out of the autoclave and dried for 12 hours.

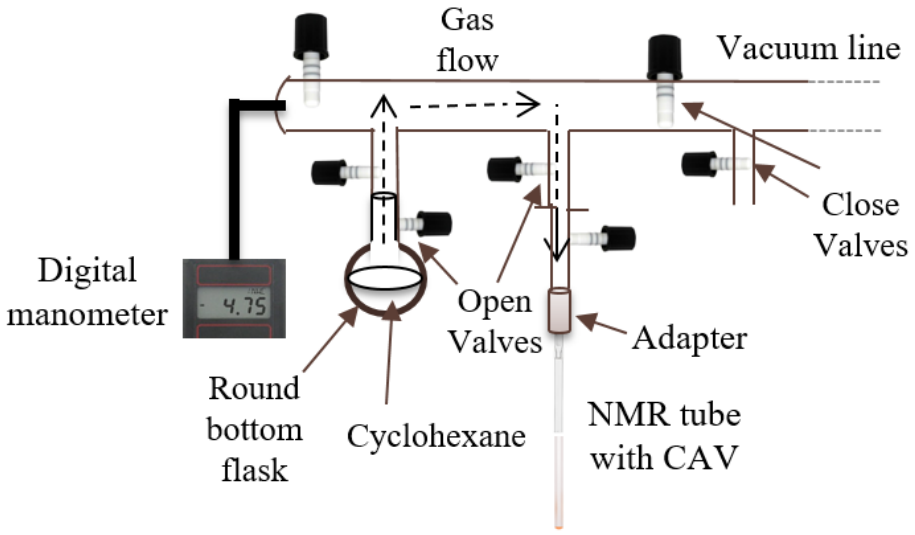

Figure 10. Schematic diagram depicting vapor flow from liquid in flask to NPG in NMR tube using vacuum line.

To start an NPG experiment, it was required that the 10-nm NPG was vacuum dried in the NMR tube by connecting it with the vacuum line using an adapter and raising the temperature up to 160˚C for 8 hours. The sample was cooled down gradually at the room temperature. After that, it was exposed to hydrocarbon, that is, cyclohexane in a controlled environment. As figure 10 portrays, one channel of vacuum line was connected to a flask containing cyclohexane and another

channel was attached to the NMR tube containing the NPG. The middle valve of the vacuum line was closed, so that no cyclohexane is vacuumed away. Due to difference in vapor pressure, the cyclohexane molecules migrated in to the nanopores of the monolith. The hydrocarbon loading within the NPGs was measure using a microbalance from Sartorius Cubis MSE that has 1μg resolution. To determine the pore fillings of the NPG, the weight of the loaded sample was compared to the dried monolith. The NMR tube with the hydrocarbon loaded NPG was then subjected to variable nitrogen pressure. Nitrogen was selected as the gas for filling the NMR tube due to its inert nature at room temperature. This to be noted that the pressure within the NMR tubes in all cases was kept to 120 psi for safety reasons.

NMR: NMR spectrometer (Bruker Avance) with 9.4 T wide-bore superconducting magnet was operated to obtain the NMR diffusion data. Specific to NMR diffusometry, 1H single-channel diffusion probe for z-gradient was used that has the gradient strengths up to 2900 gauss/cm. The NMR spectrometer is communicated through the Bruker server and a software, TopSpin that was installed in the computer with Red Hat employed on the Nvidia's kernel. Among many other techniques, the sequence stimulated echo (STE) was employed to determine the self-diffusivity coefficients. The Stejkal-Tanner equation that has been mentioned in the previous chapter expresses the signal attenuation resulting from the diffusion in STE experiment. Maximum gradient strength of applied during experiments are 180 G/cm. The diffusion observation time was varied but primarily it was 10 ms. Experiments were conducted with both 32 and 16 gradient steps to validate the accuracy. Also, the repetition times and the effective pulse-gradient length were adjusted accordingly to optimize the signal. The NMR investigations were performed at 25˚C. A chiller has been connected to the diffusion probe of the NMR to maintain the temperature at 25˚C through circulation of water around the base of the gradient coil.

CHAPTER IV

RESULTS AND DISCUSSIONS

NPG control experiments: Analysis of fluids that are present in combined phases in porous solids find application in engineering and industrial processes, including catalysis, energy investigations, and geological studies[3,119]. Thermodynamic principles are the basis of fluid behavior. The solid-fluid interaction forces control the wettability and transport characteristics within the system. Constructing a methodology that would elucidate on the mechanism of fluid mobility at nano length scale is the focus of the study. The present set of control experiments have been conducted to probe into the chemical interactions and transport behavior of the fluids confined in the complex porous structures beneath the surface of earth. The translational motion of the fluid serves as an important criterion for mapping the movement of fluid particles within porous media due to various interaction. NMR diffusometry was employed to examine the diffusion and surface interaction of water and cyclohexane in model host structures. The NPGs had a mean pore diameter of 10 nm and they were loaded with water or cyclohexane at different weight fractions and pressurized at varied magnitude with nitrogen gas.

Previously, our group have published an NMR diffusometry investigation on water/cyclohexane mixture confined in the NPG (Vycor). The key observation of the investigation was that the self-diffusion and dynamics of the mixed liquid components could not be predicted depending on how each pure liquid

behaved in confinement.[120] Figure 11 shows that the behavior for water and cyclohexane at very low loadings follows expectations for polar and hydrophobic liquids, respectively. Water exhibits a significantly smaller D_{eff} due to strong adsorption on the hydrophilic glass. On the other hand, cyclohexane shows enhanced-diffusion region relative to bulk cyclohexane due to the combined effects of surface repulsion and increased vapor pressure. Further, figure 12 depicts the selected samples spanning the composition range provide nearly the expected cyclohexane/water ratio of 1:10 based on volumes used in the sample preparation. Figure 12b shows multiple peaks from slow-exchange averaging between environments with or without the other liquid component.

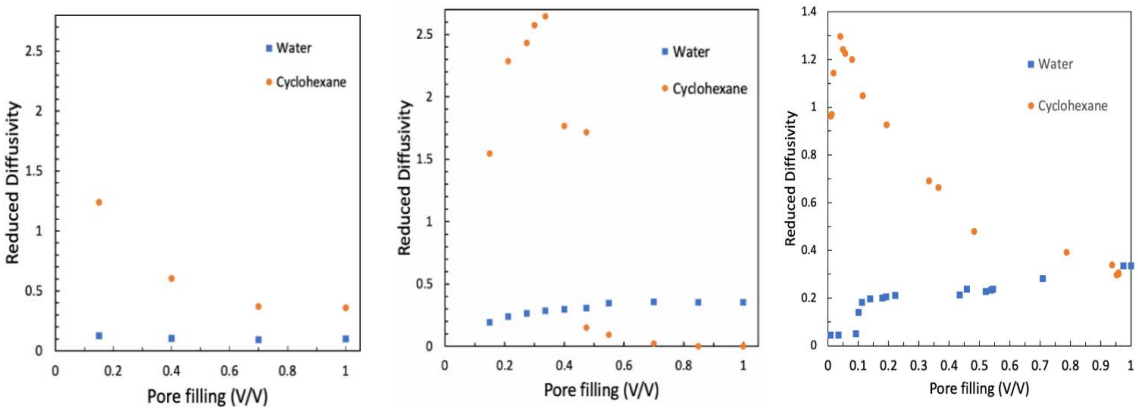

Figure 11. Reduced diffusivities ($Dapp/D_0$) of water and cyclohexane in (a) oil rich (90% v/v oil 10% v/v water), (b) water rich (10% v/v oil 90% v/v water) mixtures confined at different pore fillings in 10-nm NPG and (c) water and cyclohexane (measured separately) in confinement at different pore fillings inside 10-nm NPG. Dapp is the apparent self-diffusion coefficient and D0 is self-diffusion coefficient for the free fluid (D○ for water and cyclohexane measured separately). The effective gradient pulse duration (tg)=1 ms and diffusion time (Δ) = 50 ms. Reproduced from reference 119 with permission.

Figure 13 depicts the plots of diffusivity coefficient (m^2/s) of cyclohexane and water in the nanoporous confinement at different pore fillings inside 10-nm NPG. The self-diffusion coefficient of the fluids was measured at three different pressure levels, that is, 1 bar, 4 bar, and 8 bar of nitrogen gas. It is shown in the pictorial representation that the diffusivity of cyclohexane moves up a little till 0.04 pf the pore filling and then, continues to drop down till the pore filling is 1. Here, the observation is that there has not been any significant difference in the trend with respect to the

three different pressure magnitudes. This, in turn, indicates that the diffusivity curve follows similar trend for any pore filling below the 10 bar pressure, or in other words, the diffusion-pore filling trend is constant below 10 bar. The pore filling (V/V) of 1 was achieved by submerging the NPGs in their respective fluid bath for 24 hours and later, transferring them to the NMR tube. For pure water, there has been a gradual increase in the diffusion coefficient from 0 to 1 pore filling. Similar to cyclohexane, the diffusion-pore filling trend remains constant for any pressure magnitude below 10 bar. The diffusivity measurements were performed very less to none for the range of 0.4 to 0.9 pore volume because of requirement of long-time span for achieving the target pore filling. The challenge is the limited imbibition of the fluid in the pores and its sub-surface presence blocking the further intake of more molecules. However, the data points from pore filling 0 to 0.4 and from 0.9 to 1 shows a clear trend irrespective of the gap present.

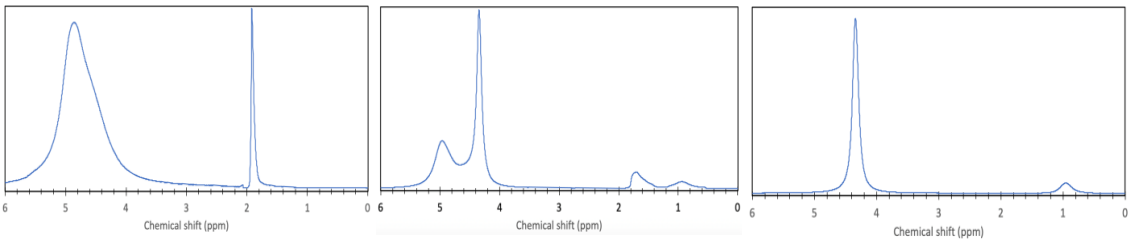

Figure 12. Effect of pore filling on chemical shift for the water-rich mixture (10/90 v/v% C6H6/H2O) confined in 10 nm nanoporous glass. a) Pore filling = 27.5%. b) Pore filling = 47.5% c) Pore filling = 85%. The C6H6/H2O peak area integrals for the 27.5, 47.5 and 85% loadings were 0.07, 0.11, 0.07 respectively. The spectra are plotted according to the intensity of the largest peak, not total area. Reproduced from reference 119 with permission.

This set of experiments were conducted to build upon the understanding of loading-dependent diffusion characteristics of the components in the host individually at varied pressure and extending it to develop the mixture measurement in the confinement or to further elevated pressure. Kimmich and coworkers have conducted experiments on crushed 4 nm Vycor NPG particles for cyclohexane and water separately[121]. Erfani et al. has reported that the partitioning of oil and water mixture confined in nanoporous geometries cannot be extrapolated from the characteristics of their separate components. They demonstrated that water adheres strongly to the

surface of Vycor NPG host of 10 nm and could cause anomalous enhanced or suppressed diffusion for the other immiscible component cyclohexane based on the pore filling. The cyclohexane was kinetically trapped in the water-rich environments[120]. In our present research work, Varapor NPGs that are inert and structurally well-defined nanoporous solid posed challenge due to their inherent chemical and physical heterogeneity. Hence, it becomes necessary to directly measure the diffusivity of each component prior to moving into mixtures or any other advancements related to complexity of the experiments.

It is important to evaluate how the non-ideal behavior of fluid mixtures is distinct from the ideal pure fluid behavior and more so, under nanoconfinement. Extending the current research work would help develop methods and techniques to analyze the fluid distribution and phase behavior in the nanoporous structures. Some specific future experiments have been discussed later in the conclusion section. The investigation will aid in the exploring the molecular dynamics and this finds application in the catalysis, energy storage, enhanced oil recovery (EOR), interfacial phenomena, colloid science, etc.

Zeolite experiments: One of the ways to control fluid interaction is to functionalize and chemically modify the surface of nanoporous media. As previously mentioned in the introduction and literature survey, the zeolite structure consists of three-dimensional networks of $[SiO_4]^{4-}$ or $[AlO_4]^{5-}$ primarily linked with O atoms connecting neighboring tetrahedra. The NMR diffusion data on CH_4 gas at 120 psi (~ 8 atm) in different type of zeolite both before and after chemical modifications shows that the diffusion coefficients are very sensitive to changes in the surface. The diffusion coefficients of pure methane and CH_4 gas in ZSM-5, zeolite Y and their modified variety are different from each other, in some cases, in the order of magnitude. The pressure of CH_4 gas was varied to assess uncertainties/fluctuations in measurements of diffusivity of the hydrocarbon in zeolite. The hydrocarbon, methane was selected as the probe molecule for it being the main component of natural gas, small size, that is, < 0.54 nm and relatively low adsorption affinity. One

of its important properties being the asymmetric exchange between a proton of the zeolite and CH_3 group, part of the CH_4, could be used as a model for C-H activation.

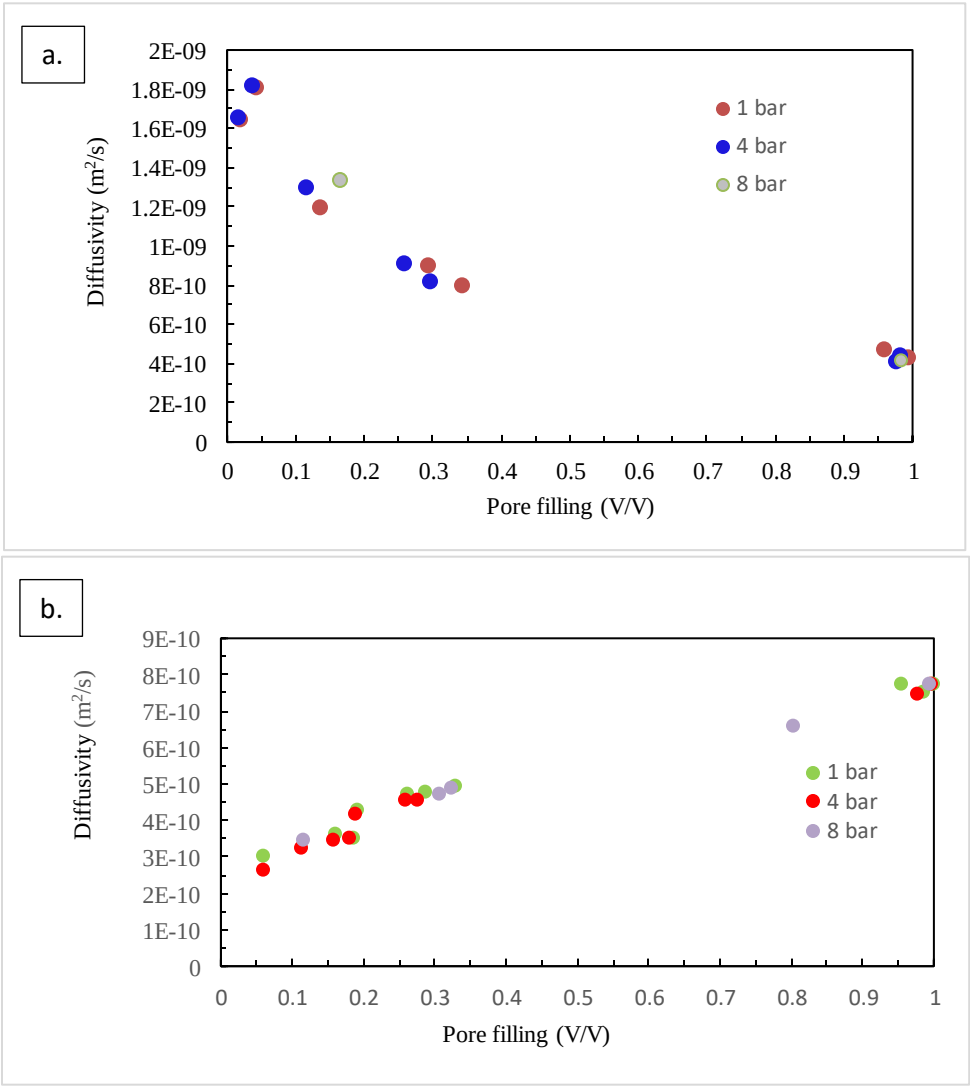

Figure 13. Diffusivities of a. cyclohexane and b. water separately in 10-nm NPG. The diffusivities are measured at three different controlled pressure of 1bar, 4 bar, and 8 bar of nitrogen gas.

Figure 14 shows a sharp and narrow ^1H NMR linewidth and shape measured through an 1D experiment on the spectrometer that indicates gaseous particles that has been traced in the nanoporous channels of ZSM-5.[122] This figure is a general representation of the chemical shifts that were observed for the 1D experiments that were conducted on the various types of zeolites. The

absence of water peak within the vicinity of the methane peak denotes that the sample is devoid of moisture to the extent that it does not show up in the NMR spectrum. The chemical environment of the proton detected on CH_4 molecule comprises of the other CH_4 molecules along with surface components of the zeolite. 1D NMR experiment was performed before each diffusion experiment to make sure that the desired composition of the sample has been achieved.

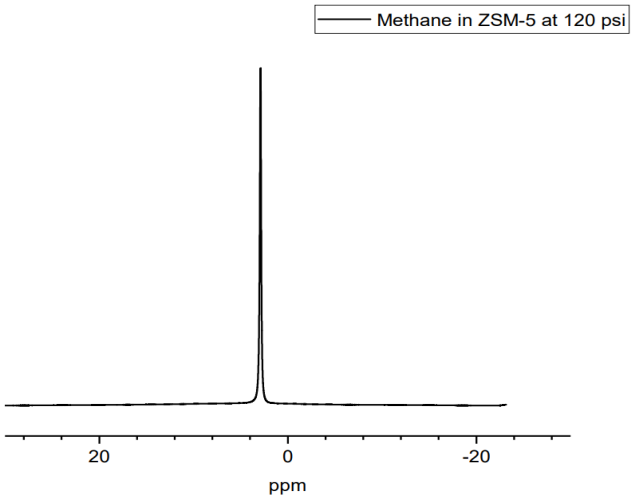

Figure 14. ^1H single-pulse NMR spectrum of CH_4 gas in H-ZSM-5 at 120 psi pressure.

Diffusion NMR techniques provide a robust and non-invasive opportunity to get chemical shifts with echo attenuation. The gradient coils produce the gradients in the magnetic field of the spectrometer for diffusion measurements, thus, it generates the pulsed field gradient in the effective sample volume. This can be explained by induced dephasing of the molecules in the sample due to the applied gradient. The diffusion of molecules in confinement is dependent on the diffusion time and the internal field gradients cause attenuation. The sequence of three 90 pulses may be advantageous in the porous media when spin-lattice relaxation time, T1 is greater than the spin-spin relaxation time, T2 as there is a dependence of the diffusion coefficient on the diffusion time. Some diffusion tests were run on liquid H_2O and D_2O control samples to check the working of the parameters set on the Topspin software. The results yielded diffusion coefficient in the range of

$1.8x10^{-9}$ to $2.3x10^{-9}$ m^2/s for the H_2O/D_2O samples. This confirms valid operating parameters as the data matches the values mentioned in the literature.[123]

It is essential to calibrate the experiment for implementation of accurate methods and garner valid data. Each set of experiment, that includes vacuum drying the zeolite and then running NMR experiment, was repeated few times to check the reproducibility of the data. Repeating the experiments aided in assessing the deviations in measurements and that provided a necessary platform to analyze the uncertainties associated with the methods. Also, it has facilitated the identification of certain issues and their solution, such as, addition of sonication to eliminate any clusters or extra-space within the effective sample volume. Table 1 and figure 15a demonstrates the error associated with the measurement of diffusion coefficient of pure methane, that is, methane without any constraints other than the wall of NMR tube. The error bars were reported to show confidence of reproducibility. The data was collected few times, 3 to 5 times in general, to find the average value and the standard deviation associated with the measurements. The standard deviation was determined through the formula:

$$\sigma = \sqrt{\frac{\Sigma(x_i - \bar{x})^2}{n-1}} \quad \ldots(14)$$

In the above formula, $\bar{x}$ is the sample mean in the n sample size.[124] The figure shows that the diffusivity coefficient has higher error at 4 atm than that in the rest two values, 6 atm and 8 atm. This error may not be of any relevance to the structure of the zeolites but it could be a sensitivity issue, that is, signal-to-noise ratio arising for shorter T2 relaxation. Another important observation to note here is that the diffusion coefficient of pure methane decreases with increasing the pressure. As the pressure increases, the molecules of methane come closer of each other and the density increases. The movements of the molecules get restricted to a great extent. The values of the diffusion coefficients remain in the same order of magnitude irrespective of the pressure applied,

which is within the range of 4 atm to 8 atm. Figure 15b displays the plot for diffusion coefficient versus diffusion time for pure methane and methane in HY and its rare-earth counterparts. The nX and mC that are used in denoting LaY nXmC which stand for the number of ion-exchanges and calcinations, respectively. The graph shows that for diffusion time of 10 to 400 ms, the diffusion coefficients of pure methane remains the same and appears to be comparably a straight line. The small decrease that is observed in diffusion coefficient with diffusion time, big delta Δ could be attributed to either the hindrance provided by the heterogeneous environment in the nanoporous channels or very short T2 relaxation time.

Table 1. Pressure (atm), diffusivity coefficient (m^2/s) and standard deviation for pure methane gas. The diffusion time is 10 ms.

Pressure (atm)	Diffusivity Coefficient (m^2/s)	Std. deviation
8	2.439E-06	±4.35408E-08
6	2.921E-06	±1.74986E-08
4	3.845E-06	±1.62388E-07

Table 2 and figure 16a shows that the diffusion coefficient of commercial NH_4^+-ZSM-5 that was as received from the supplier without calcination or any modification. It follows that same trend where the diffusivity reduces with increase in pressure. Although there is an anomaly with the average diffusion coefficient of NH_4^+-ZSM-5 at 6 atm and 8 atm, we can consider that to be an error as possible collection of more data will show the trend to be as expected. Moreover, there are data points with less diffusion coefficient value than that of the lowest valve at 6 atm. It is important to note that the diffusivity coefficients of the Si/Al = 40 in this case are less than that

found for Si/Al = 15 for each pressure measurements. Table 3 and figure 16b displays that the diffusivity coefficient of H-ZSM-5 with Si/Al = 15 is lower than that of H-ZSM-5 with Si/Al = 40. The error associated with the diffusivity of H-ZSM-5 with Si/Al = 40 is quite high.

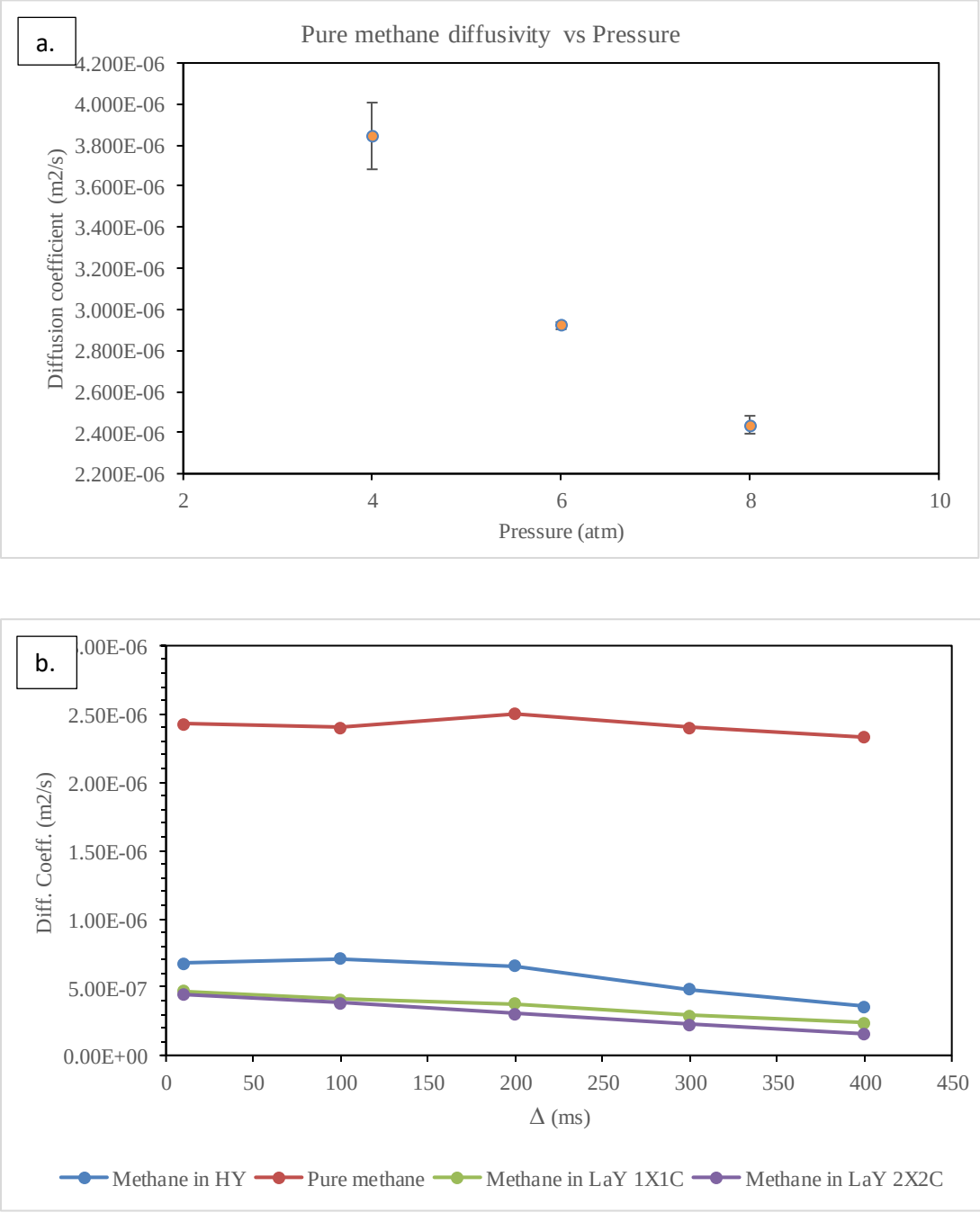

Figure 15. a. Plot for Diffusivities (m^2/s) vs. Pressure (atm) of pure methane gas. The diffusion time is 10 ms. The error bars are plotted as one standard deviation. b. Diffusivity (m^2/s) vs. diffusion time Δ (ms) for pure methane, methane in HY and its La modified counterparts LaY 1X1C and LaY 2X2C.

Table 2. Pressure (atm), diffusivity coefficient (m^2/s) and standard deviation for methane gas in NH4-ZSM-5 Si/Al= 15 & Si/Al = 40. The diffusion time is 10 ms.

	NH_4^+-ZSM-5 Si/Al =15		NH_4^+-ZSM-5 Si/Al =40	
Pressure (atm)	Diffusivity Coefficient (m^2/s)	Std. deviation	Diffusivity Coefficient (m^2/s)	Std. deviation
4	7.59E-07	±2.68027E-08	4.08E-07	±4.1156E-08
6	6.25E-07	±2.73904E-08	3.76E-07	±4.15006E-08
8	6.40E-07	±4.46027E-08	3.32E-07	±3.89288E-08

Table 3. Diffusivity coefficient (m^2/s) and standard deviation for methane gas in H-ZSM-5 Si/Al= 15 & Si/Al = 40. The diffusion time is 10 ms.

Zeolite type	Diffusivity Coefficient (m^2/s)	Std. deviation
HZSM-5 Si/Al = 15	2.99E-07	±6.14356E-09
HZSM-5 Si/Al = 40	7.56E-07	±4.6775E-07

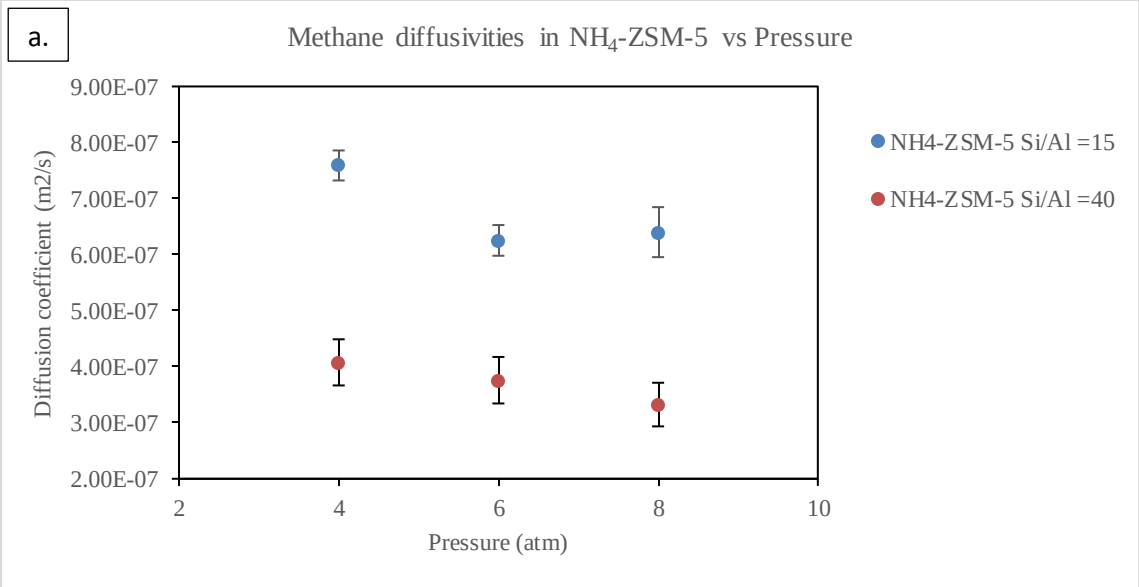

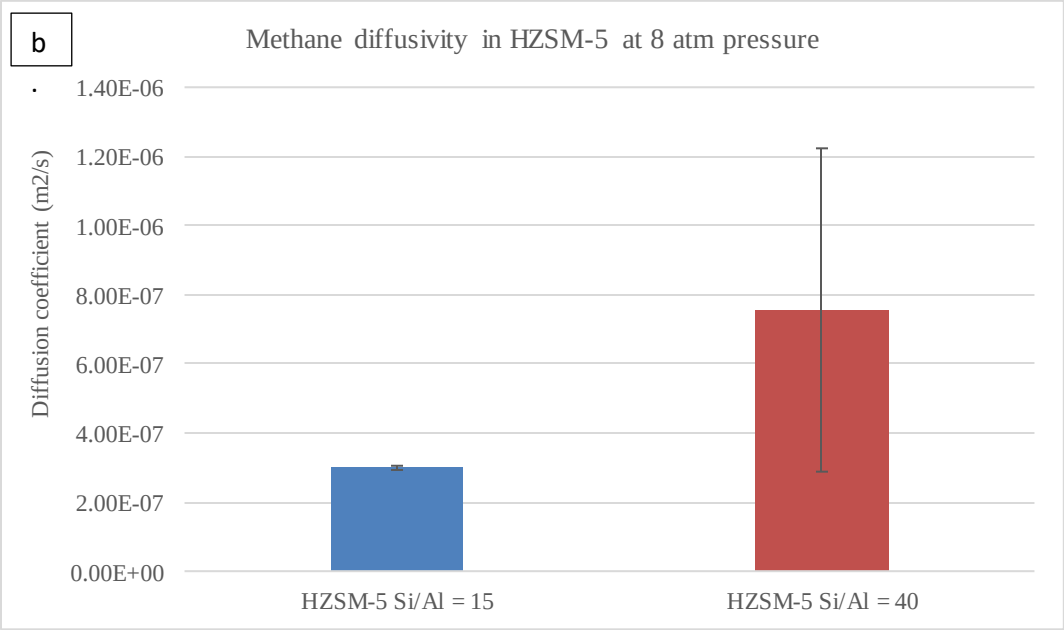

Figure 16. a. Plot for Diffusivities (m^2/s) vs. Pressure (atm) for NH4-ZSM-5 Si/Al= 15 & Si/Al = 40 and b. Diffusivities (m^2/s) of methane with standard error bars in H-ZSM-5 with Si/Al of 15 and 40. The diffusion time is 10 ms. The error bars are plotted as one standard deviation.

Figure 17 shows the NMR diffusion data for the control experiments on zeolite with methane, in which the linearized raw echo attenuation is a function of g^2 with STE method. The plot of signal intensity vs g^2 for HZSM-5 depicts that the intensity drops as the gradient strength was increased. The Stejskal-Tanner equation was used to verify the output provided by the

software. The diffusion coefficient calculated by the software was equal to 2.92×10^{-7} m^2/s for 32 gradient steps whereas the manually calculated value was found to be 2.89×10^{-7} m^2/s. Similarly, the plot of signal vs intensity for ZSM-5 AHFS washed sample has confirmed that the value was 1.41×10^{-7} m^2/s compared to 1.39×10^{-7} m^2/s for 32 gradient steps which was displayed by the software. The ZSM-5 that was used for both the experiments has the Si/Al of 15.

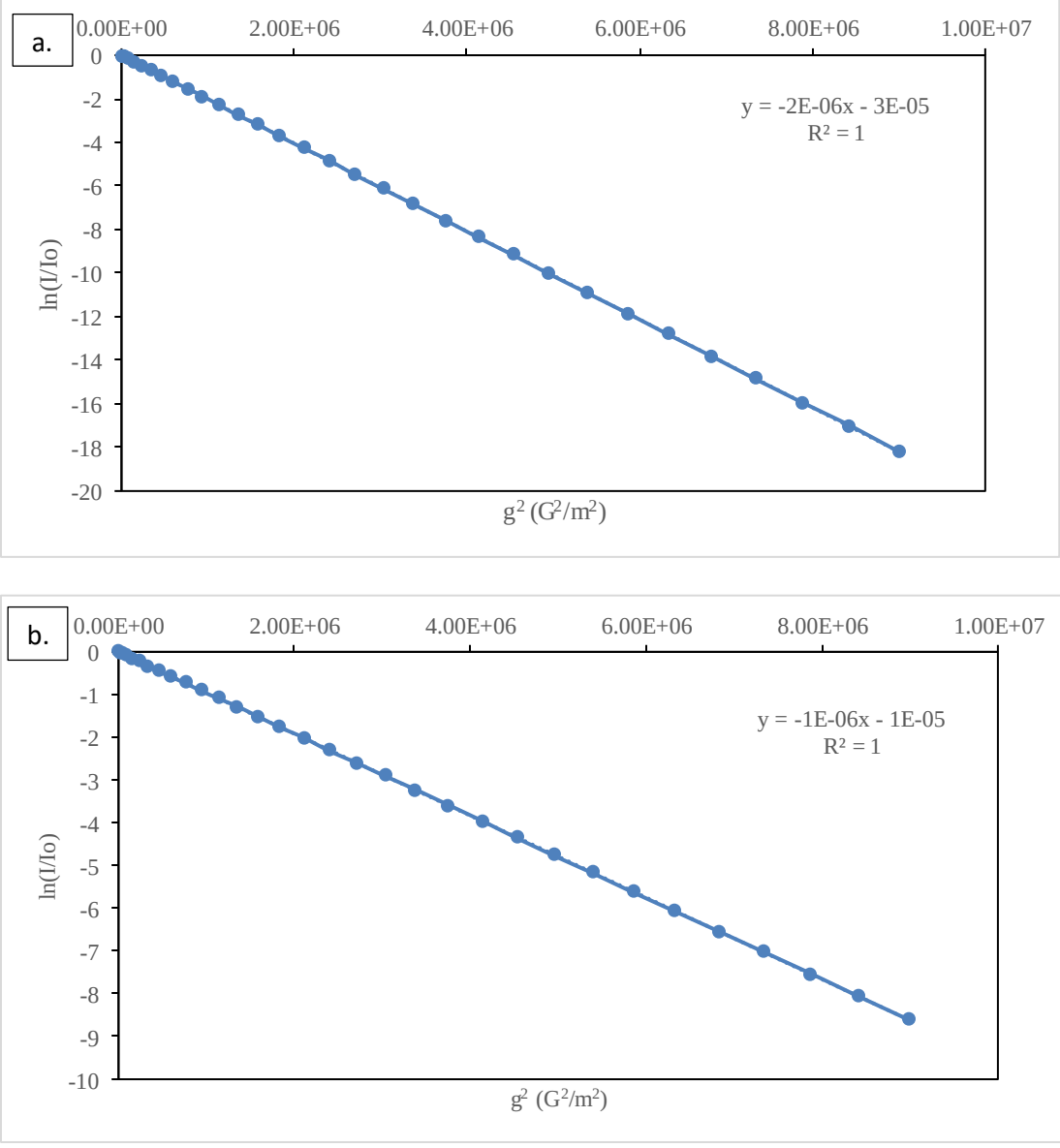

Figure 17. Plots of signal intensity vs. gradient strength square (G^2/m^2) for a variety of a. HZSM-5 Si/Al = 15 and b. AHFS washed ZSM-5 Si/Al = 15. The diffusion time is 10 ms.

Figure 18 is the pictorial representation of ln(I/Io) versus square of gradient strength graph. Here, steeper the slope, the greater is the diffusivity of the zeolite type. The different Si/Al ratios of zeolite was taken and deammoniated to get the diffusion coefficient of the protonated form of zeolite. A trend can be observed with respect to the Si/Al ratio, that is, the slopes get steeper with increasing Si/Al ratio of the ZSM-5, except for Si/Al = 140. The AHFS washing was carried out to remove the extraframework aluminum (EFAl) from the zeolite structure.[125] The EFAl species contribute to Bronsted acid sites, thus impacting the catalytic activity and selectivity in zeolites. Counterintuitive to getting a steeper slope for the AHFS WASHED ZSM-5, their diffusion coefficient was found to be comparatively quite low than the other zeolite. AHFS washing could have caused loss in crystallinity, the lower diffusion coefficient may have been a consequence of that.

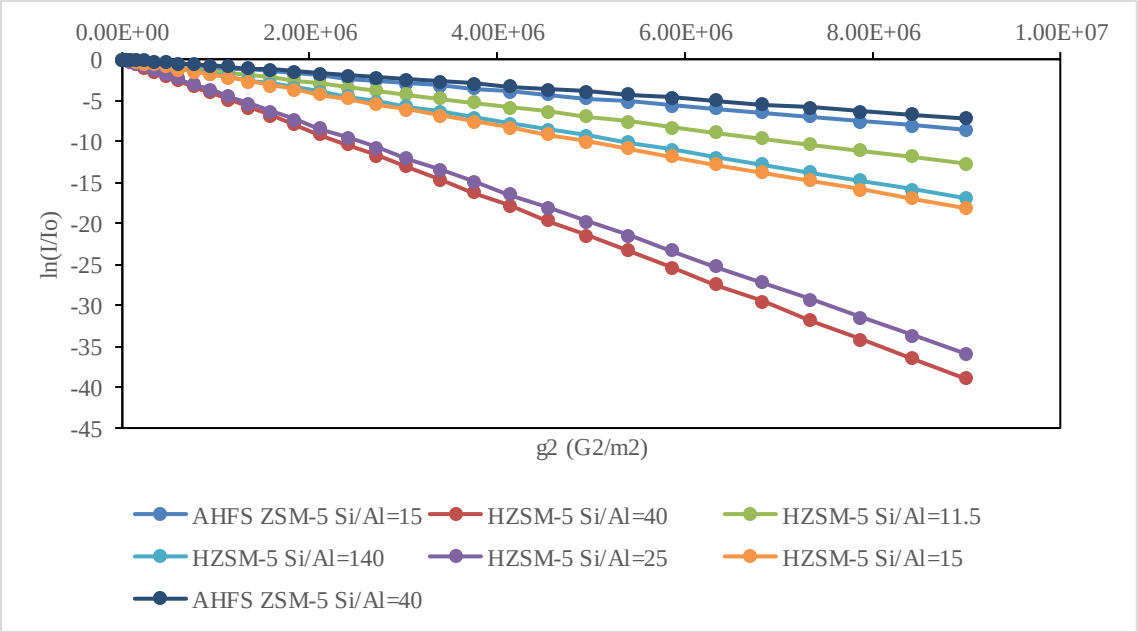

Figure 18. Plot of signal intensity vs. gradient strength square (G^2/m^2) for a variety of ZSM-5 catalysts as indicated. The diffusion time is 10 ms.

The table 4 shows the diffusivity coefficients and root mean square displacement R values for the ZSM-5 with different Si/Al ratios and their modified counterparts. The H-ZSM-5 with Si/Al

= 15 and 40 have been taken as a representation for MFI low Si/Al and high Si/Al, respectively. They were considered for the various modifications, such as AHFS treatment, phosphoric acid treatment and steaming. The phosphoric acid treatment is believed to impart hydrothermal stability to the catalyst framework structure. Hence, the diffusion coefficient for P-ZSM-5 Si/Al =15 has decreased to $8x10^{-8}$ m^2/s from the $2.92x10^{-7}$ m^2/s for the protonated form. Similarly, the diffusion coefficient of P-ZSM-5 Si/Al = 40 has dropped to $1.27x10^{-7}$ m^2/s from the value of $6.27x10^{-7}$ m^2/s for its H-counterpart. The two different steaming methods were applied to HZSM-5. The water bubbler method did not show any difference in diffusion coefficient whereas the autoclave method showed a decrease in diffusion coefficient for both Si/Al ratios of 15 and 40. This indicated a loss of crystallinity in the zeolite structure due to steaming through autoclave method.[118] So, the autoclave steaming of H-ZSM-5 lead to dealumination and formation of extraframework Al species.

Although there are reports on diffusion in zeolite that did not acknowledge that uncertainty involved in the variable pressure/concentration measurements such as diffusion of methane in CHA-zeolite,[126] some recent research works have considered pressure uncertainty/error bars that were performed on ZIFs. Vasenkov et al. have conducted NMR studies of the self-diffusion of individual gases including carbon dioxide, methane, ethylene, ethane, and xenon as well as selected mixture of two-components in ZIF-8 and ZIF-7-8 crystals. They have considered all D_{eff} c/p values with an uncertainty of 40%. The pressure above the ZIF bed has been kept to a maximum of 9 bar for the different gases. The primary observations include indication of increased influence of the framework flexibility on diffusion in ZIF-7-8 relative to ZIF-8 and for gases larger than carbon dioxide, the diffusivity ratios ZIF-8 and ZIF-7-8 do not elevate with increasing gas size at any of the loading pressures.[127] Similar study on variable gas pressure was performed on ZIF-11 crystals by the Vasenkov's group to investigate the intracrystalline regime. They obtained an anomalous relationship between sorbate size and diffusivity that shows an effect of ethylene/framework

interaction can be a reduction in the linker flexibility that reduces the maximum and/or effective aperture size in ZIF-11.[128]

Table 4. Diffusivity coefficient (m^2/s), $<R^2>$ (m^2) and root mean square displacement R (m) for methane gas in a variety of ZSM-5. The diffusion time is 10 ms.

Type	Diffusivity Coefficient (m^2/s)	$<R^2>$ (m^2)	Root mean square displacement R (m)
HZSM-5 (Si/Al = 11.5)	2.05E-07	1.23E-08	1.11E-04
HZSM-5 (Si/Al =15)	2.92E-07	1.75E-08	1.32E-04
HZSM-5 (Si/Al =25)	5.78E-07	3.47E-08	1.86E-04
HZSM-5 (Si/Al =40)	6.27E-07	3.76E-08	1.94E-04
HZSM-5 (Si/Al =140)	2.73E-07	1.64E-08	1.28E-04
ZSM-5 (Si/Al =15) AHFS washed	1.39E-07	8.31E-09	9.12E-05
ZSM-5 (Si/Al =40) AHFS washed	1.16E-07	6.98E-09	8.36E-05
PZSM-5 (15) (P/Al = 1:1)	8.004E-08	4.80E-09	6.93E-05
PZSM-5 (40) (P/Al = 1:1)	1.266E-07	7.60E-09	8.72E-05
Steamed H-ZSM-5 (Si/Al = 15) water bubbler method	2.98E-07	1.79E-08	1.34E-04
Steamed H-ZSM-5 (Si/Al = 15) autoclave method	1.29E-07	7.72E-09	8.79E-05
Steamed H-ZSM-5 (Si/Al = 40) autoclave method	9.14E-08	5.48E-09	7.41E-05

Table 5 and figure 19 show that the H-ZSM-5 has higher diffusion coefficient than that of P-ZSM-5 and the error is quite low for both. The method that was used to introduce phosphorus atoms to the zeolite framework is referred to as wet incipient impregnation method. Addition of P to ZSM-5 leads to improved selectivity and hydrothermal stability.[129] In this research, the P/Al =

1:1 was prepared for taking the measurements and effect of changes in ratio is needed to be investigated for further insights.

Table 5. Diffusivity coefficient (m^2/s) and standard deviation for methane gas in H-ZSM-5 Si/Al= 15 and PZSM-5 Si/Al = 15 (P/Al = 1:1). The diffusion time is 10 ms.

Zeolite type	Diffusivity Coefficient (m^2/s)	Std. deviation
HZSM-5 Si/Al = 15	2.99E-07	±6.14356E-09
PZSM-5 Si/Al = 15 (P/Al = 1:1)	8.12E-08	±7.64936E-09

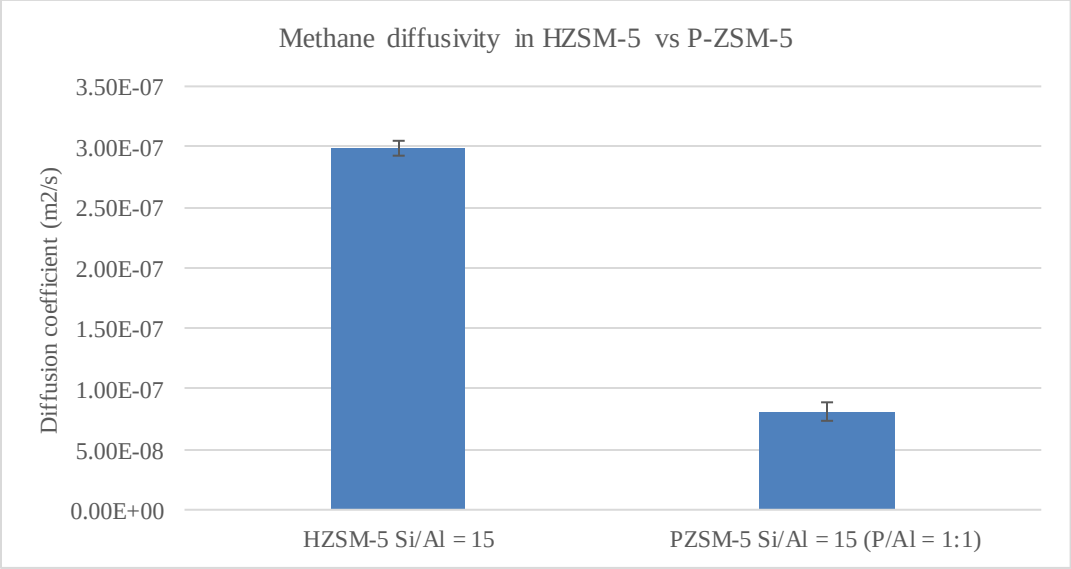

Figure 19. Diffusivities (m^2/s) of methane with standard error bars in H-ZSM-5 and P-ZSM-5 (P/Al = 1:1) with Si/Al = 15. The diffusion time is 10 ms. The error bars are plotted as one standard deviation.

The table 6 and figure 20 shows that the diffusion coefficient of methane in HY decreases when ion exchange occurs with rare-earth ion and the vacuum drying step follows. It indicates that the La^{3+} exchange caused removal of aluminum from framework and presence of the ion that could be trapped in the cages, thus, mobility of methane reduces.[130] The modification of HY with rare-earth salts has been considered to increase the stability in presence of water.[131] The difference in root mean square displacement between the LaY 1X1C and 2X2C is very little. The exchange of

La^{3+} with zeolite for once is effective for diffusion purposes. Although figure points to the fact that the deviation for diffusion coefficient of methane in LaY is high, it stays relatively lower than the mean diffusion coefficient of methane in HY. One data point of HY has been discarded from the calculation as it is only data that is an order of magnitude higher than the rest of the values and can be considered as an outlier.

Table 6. Diffusivity coefficient (m^2/s), $<R^2>$ (m^2) and root mean square displacement R (m) for methane gas in HY, LaY 1X1C and LaY 2X2C. The diffusion time is 10 ms.

Type	Diffusivity Coefficient (m^2/s)	$<R^2>$ (m^2)	Root mean square displacement R (m)
HY	7.39E-07	4.43E-08	2.11E-04
LaY 1X1C	4.69E-07	2.82E-08	1.68E-04
LaY 2X2C	4.46E-07	2.68E-08	1.64E-04

An important application of variable pressure work on gases encompasses hydrogen storage. Various porous materials such as clay minerals, zeolites, and metal–organic framework materials are used as an alternative to store hydrogen. The H_2 uptake usually ranges from 0 to 2 weight % with pressure range of 0-1.5 MPa. The main factors that influences the amount of hydrogen adsorbed are the framework structure, the composition, and the nature of the zeolite.[132–134] Chen et al. have designed and prepared Ru single-atoms catalyst supported on *BEA zeolite (Beta) for hydrogen storage. They observed that the obtained Ru(Na)/Beta catalyst exhibits excellent activity in the hydrogenation of N-ethylcarbazole with the hydrogen uptake of 5.69 wt. % and a conversion rate of > 99% within 1.5 h for the 6 MPa H_2 at 100 °C.[135]

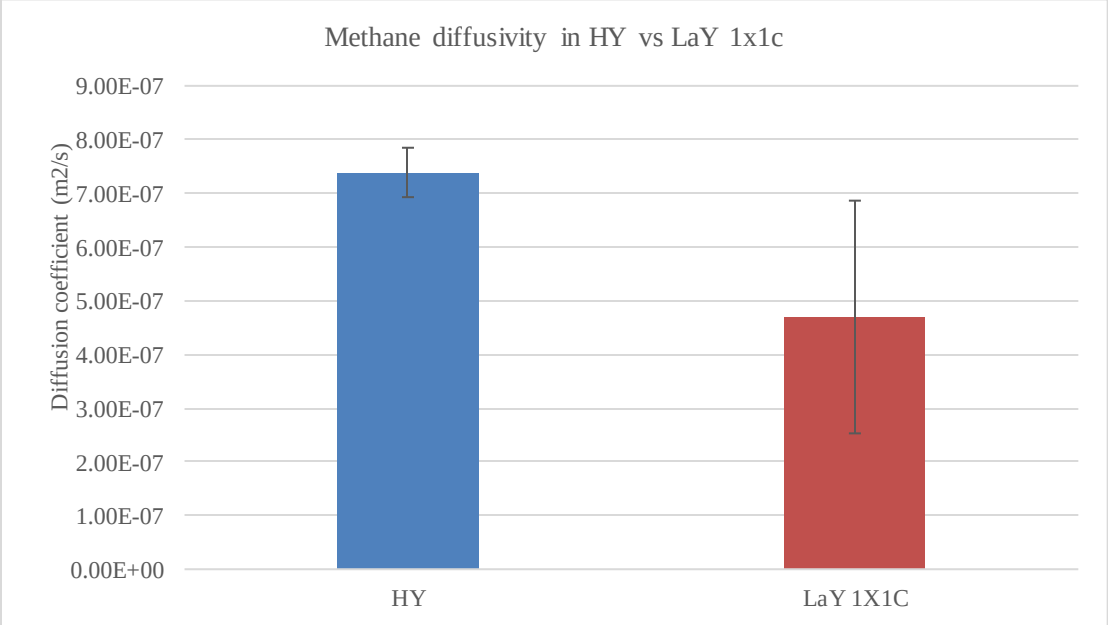

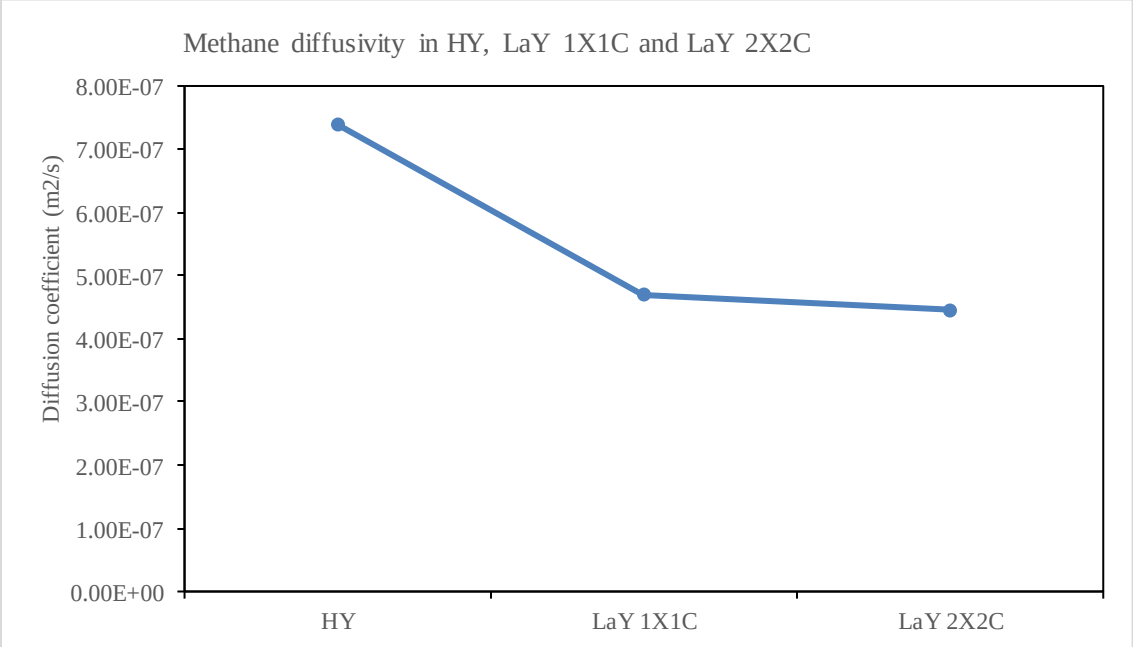

Figure 20. a. Diffusivities (m^2/s) of methane with standard error bars in HY and LaY 1X1C. b. Diffusivities of methane in HY, LaY 1X1C and LaY 2X2C. The diffusion time is 10 ms. The error bars are plotted as one standard deviation.

CHAPTER V

CONCLUSIONS AND FUTURE DIRECTIONS

The contribution of NMR diffusometry in studying the transport behavior of molecules in nanoporous media is paramount. The self-diffusivity coefficient is a gateway to embark on the journey to explore the interaction that occurs between fluid particles and the surface of the solid. It is a domain that has been the focus of interest of the scientific community and the advancements demonstrate that it is heading the right way. This specific research is conducted to understand the diffusion of hydrocarbons, oil and water characteristics in the nanoporous hosts, NPGs and zeolite. The water and cyclohexane diffusivity in the NPG under nitrogen pressure demonstrated that mobility remain the same at any pressure below 10 atm. While there is an increase in diffusion coefficient of water with the pore filling from 0 to 1 at that pressure range, the cyclohexane diffusivity coefficient displays an increase from 0 to 0.04 pore volume and then gradually decrease till 1. Further exploration on diffusivity of water and cyclohexane at higher pressure range of 1000 to 10000 psi is necessary to emulate the pressure condition beneath the surface of earth. The other factors that could aid in the investigation are the presence of surfactants and/or surface functionalization. The chemical shift resolution of NMR spectrometry bestows the ability to measure such changes in the transport of the fluids. Altering the pore size of the NPGs, different oil-water mixture and the gas used for pressurizing the NMR tubes could be another way the research can progress.

The collection and analysis of diffusion data through NMR spectrometry have facilitated gaining some insights on diffusion in ZSM-5 and zeolite Y. These insights elucidate on how hydrocarbons behave in a variety of modified zeolites. Some zeolites such as H-ZSM-5 with Si/Al = 15 show the highest stability with respect to reproducibility of self-diffusion coefficient while others such as H-ZSM-5 Si/Al = 40 and rare-earth modified HY have displayed extended deviation on repeating the set of data. The errors could be a function of both the complexity of the structure of zeolite and design faults of the NMR tube that causes pressure uncertainties. Large number of control experiments needs to be conducted to underpin the major cause of the errors. Although the diffusion experiments were conducted at diffusion time set to 10 ms, more examination is required to understand the effect of varying the diffusion time that changes the diffusivity. Different diffusion trends of methane in zeolites have been identified in our research work and they have the possibility to find applicability in the catalysis, adsorption and ion exchange industry. It was confirmed through the experiments that diffusion coefficient of pure methane and methane in zeolites decrease with increase in pressure. Performing the experiments at different temperature will allow quantification of activation energy of diffusion. Future experiments of NMR diffusometry on the steamed HY, BEA zeolite and silicalite can be conducted. Another set of experiments can be performed to investigate the effect of varied P/Al ratios in the zeolite framework. The chemically modified zeolites can be used to predict diffusion behavior of oxygen, nitrogen, carbon dioxide and methane for the pressure-swing adsorption systems.[136]

One of the primary outcomes of this work is a method that has been developed for introducing gases into nanoporous solids at variable pressure and it yields highly reproducible diffusion coefficients. The technique allows preparing samples in an NMR tube that can be sealed after the introduction of the gas and made ready for NMR diffusometry experiments. This particular process of introducing gases at variable pressure has shown consistent results with respect to reproducibility. Repeating the experiments aided in determining the deviations in measurements

and therefore, analyze the uncertainties associated with the method. The standard deviation, 1σ was established for the entire process and it is a significant outcome, considering that there is not enough mention of similar work in the literature. Hence, this contribution will enable the scientific community and the industry in general to explore diffusion studies on other albeit similar systems with confidence.

Diffusion of fluids under nanoconfinement is an area that has enormous scope for exploration. Ongoing investigation on the optimization of each process has led to the progress of various aspects associated with the industries mentioned previously. Zeolites and NPG's are key model systems to further understanding of how gases and liquids adsorb, diffuse, and partition in nanoporous solids. It is important that these nanoporous structures can be modified and tailored in so many ways to meet the necessity. Identification and application of the diffusion trends in the industry would pave a way to optimize the processes. It will facilitate the optimization of energy costs in industries involved with this area of research and hence, boost the economy and improve our daily lives.

REFERENCES

(1) Shewmon, P. High Diffusivity Paths. In Diffusion in Solids; Springer International Publishing: Cham, 2016; pp 189–222. https://doi.org/10.1007/978-3-319-48206-4_6.

(2) Kärger, J.; Ruthven, D. M. Diffusion in Zeolites. Comparison of Sorption and Nuclear Magnetic Resonance Diffusivities. J. Chem. Soc. Faraday Trans. 1 Phys. Chem. Condens. Phases **1981**, 77 (7), 1485. https://doi.org/10.1039/f19817701485.

(3) Ray, M. S. Diffusion in Zeolites and Other Microporous Solids, by J. Karger and D. M. Ruthven, John Wiley, New York, USA (1992). 605 Pages. ISBN 0-47 1-50907-8. Dev. Chem. Eng. Miner. Process. **2008**, 4 (3–4), 254–254. https://doi.org/10.1002/apj.5500040311.

(4) Jacobs, M. H. Diffusion Processes; Springer Berlin Heidelberg: Berlin, Heidelberg, 1967. https://doi.org/10.1007/978-3-642-86414-8.

(5) Vaughan, D. E. W. Zeolites and Other Microporous Materials. In Studies in Surface Science and Catalysis; Elsevier, 1989; Vol. 49, pp 95–116. https://doi.org/10.1016/S0167-2991(08)61710-3.

(6) Zeolite Molecular Sieves: Structure, Chemistry, and Use D. W. Breck (Union Carbide Corporation, Tarrytown, New York) John Wiley and Sons, New York, London, Sydney, and Toronto. 1974. 771 Pp. $11.95. J. Chromatogr. Sci. **1975**, 13 (4), 18A-18A. https://doi.org/10.1093/chromsci/13.4.18A-c.

(7) Karger, J.; Ruthven, D. M. On the Comparison between Macroscopic and n.m.r. Measurements of Intracrystalline Diffusion in Zeolites. Zeolites **1989**, 9 (4), 267–281. https://doi.org/10.1016/0144-2449(89)90071-7.

(8) Price, W. S. NMR Studies of Translational Motion: Principles and Applications, 1st ed.; Cambridge University Press, 2009. https://doi.org/10.1017/CBO9780511770487.

(9) Hrabe, J.; Kaur, G.; Guilfoyle, D. Principles and Limitations of NMR Diffusion Measurements. J. Med. Phys. **2007**, 32 (1), 34. https://doi.org/10.4103/0971-6203.31148.

(10) Han, K. N.; Bernardi, S.; Wang, L.; Searles, D. J. Water Diffusion in Zeolite Membranes: Molecular Dynamics Studies on Effects of Water Loading and Thermostat. J. Membr. Sci. **2015**, 495, 322–333. https://doi.org/10.1016/j.memsci.2015.08.033.

(11) Shakhgil'dyan, G. Yu.; Piyanzina, K. I.; Stepko, A. A.; Natyrov, A. N.; Mikhailov, A. M.; Savinkov, V. I.; Sigaev, V. N. Nanoporous Glass with Controlled Pore Size for High-Efficiency Synthesis of Oligonucleotides. Glass Ceram. 2019, 75 (9–10), 377–382. https://doi.org/10.1007/s10717-019-00089-3.

(12) Connolly, E. J.; Pham, H. T. M.; Groeneweg, J.; Sarro, P. M.; French, P. J. Relative Humidity Sensors Using Porous SiC Membranes and Al Electrodes. Sens. Actuators B Chem. 2004, 100 (1–2), 216–220. https://doi.org/10.1016/j.snb.2003.12.064.

(13) Maesen, T.; Marcus, B. Chapter 1 The Zeolite Scene—An Overview. In Studies in Surface Science and Catalysis; Elsevier, 2001; Vol. 137, pp 1–9. https://doi.org/10.1016/S0167-2991(01)80242-1.

(14) Li, Y.; Yu, J. Emerging Applications of Zeolites in Catalysis, Separation and Host–Guest Assembly. Nat. Rev. Mater. 2021, 6 (12), 1156–1174. https://doi.org/10.1038/s41578-021-00347-3.

(15) Ramesh, K.; Reddy, D. D. Zeolites and Their Potential Uses in Agriculture. In Advances in Agronomy; Elsevier, 2011; Vol. 113, pp 219–241. https://doi.org/10.1016/B978-0-12-386473-4.00004-X.

(16) Jiang, N.; Shang, R.; Heijman, S. G. J.; Rietveld, L. C. High-Silica Zeolites for Adsorption of Organic Micro-Pollutants in Water Treatment: A Review. Water Res. 2018, 144, 145–161. https://doi.org/10.1016/j.watres.2018.07.017.

(17) Cihan, A.; Tokunaga, T. K.; Birkholzer, J. T. Diffusion-to-Imbibition Transition in Water Sorption in Nanoporous Media: Theoretical Studies. Water Resour. Res. 2021, 57 (6). https://doi.org/10.1029/2021WR029720.

(18) Bingre, R.; Louis, B.; Nguyen, P. An Overview on Zeolite Shaping Technology and Solutions to Overcome Diffusion Limitations. Catalysts 2018, 8 (4), 163. https://doi.org/10.3390/catal8040163.

(19) Auerbach, S. M.; Carrado, K. A.; Dutta, P. K. Handbook of Zeolite Science and Technology, 0 ed.; CRC Press, 2003. https://doi.org/10.1201/9780203911167.

(20) Valdés, M. G.; Pérez-Cordoves, A. I.; Díaz-García, M. E. Zeolites and Zeolite-Based Materials in Analytical Chemistry. TrAC Trends Anal. Chem. 2006, 25 (1), 24–30. https://doi.org/10.1016/j.trac.2005.04.016.

(21) Yi, X.; Liu, K.; Chen, W.; Li, J.; Xu, S.; Li, C.; Xiao, Y.; Liu, H.; Guo, X.; Liu, S.-B.; Zheng, A. Origin and Structural Characteristics of Tri-Coordinated Extra-Framework Aluminum Species in Dealuminated Zeolites. J. Am. Chem. Soc. 2018, 140 (34), 10764–10774. https://doi.org/10.1021/jacs.8b04819.

(22) Zhang, Q.; Gao, S.; Yu, J. Metal Sites in Zeolites: Synthesis, Characterization, and Catalysis. Chem. Rev. 2022, acs.chemrev.2c00315. https://doi.org/10.1021/acs.chemrev.2c00315.

(23) Krishna, R.; van Baten, J. M. Diffusion of Hydrocarbon Mixtures in MFI Zeolite: Influence of Intersection Blocking. Chem. Eng. J. 2008, 140 (1–3), 614–620. https://doi.org/10.1016/j.cej.2007.11.026.

(24) Sultana Poly, S.; Hakim Siddiki, S. M. A.; Touchy, A. S.; Yasumura, S.; Toyao, T.; Maeno, Z.; Shimizu, K. High-Silica Hβ Zeolites for Catalytic Hydration of Hydrophobic Epoxides and Alkynes in Water. J. Catal. 2018, 368, 145–154. https://doi.org/10.1016/j.jcat.2018.10.004.

(25) Xiao, J.; Wei, J. Diffusion Mechanism of Hydrocarbons in Zeolites—II. Analysis of Experimental Observations. Chem. Eng. Sci. 1992, 47 (5), 1143–1159. https://doi.org/10.1016/0009-2509(92)80237-7.

(26) Yu, Z.; Li, S.; Wang, Q.; Zheng, A.; Jun, X.; Chen, L.; Deng, F. Brønsted/Lewis Acid Synergy in H–ZSM-5 and H–MOR Zeolites Studied by 1 H and 27 Al DQ-MAS Solid-State NMR Spectroscopy. J. Phys. Chem. C 2011, 115 (45), 22320–22327. https://doi.org/10.1021/jp203923z.

(27) Almutairi, S. M. T.; Mezari, B.; Filonenko, G. A.; Magusin, P. C. M. M.; Rigutto, M. S.; Pidko, E. A.; Hensen, E. J. M. Influence of Extraframework Aluminum on the Brønsted Acidity and Catalytic Reactivity of Faujasite Zeolite. ChemCatChem 2013, 5 (2), 452–466. https://doi.org/10.1002/cctc.201200612.

(28) Lakiss, L.; Ngoye, F.; Canaff, C.; Laforge, S.; Pouilloux, Y.; Qin, Z.; Tarighi, M.; Thomas, K.; Valtchev, V.; Vicente, A.; Pinard, L.; Gilson, J.-P.; Fernandez, C. On the Remarkable Resistance to Coke Formation of Nanometer-Sized and Hierarchical MFI Zeolites during Ethanol to Hydrocarbons Transformation. J. Catal. 2015, 328, 165–172. https://doi.org/10.1016/j.jcat.2014.12.030.

(29) Hartmann, M.; Machoke, A. G.; Schwieger, W. Catalytic Test Reactions for the Evaluation of Hierarchical Zeolites. Chem. Soc. Rev. 2016, 45 (12), 3313–3330. https://doi.org/10.1039/C5CS00935A.

(30) Holm, M. S.; Taarning, E.; Egeblad, K.; Christensen, C. H. Catalysis with Hierarchical Zeolites. Catal. Today 2011, 168 (1), 3–16. https://doi.org/10.1016/j.cattod.2011.01.007.

(31) Schroeder, C.; Hansen, M. R.; Koller, H. Ultrastabilization of Zeolite Y Transforms Brønsted-Brønsted Acid Pairs into Brønsted-Lewis Acid Pairs. Angew. Chem. Int. Ed. 2018, 57 (43), 14281–14285. https://doi.org/10.1002/anie.201808395.

(32) Kärger, J.; Pfeifer, H.; Rauscher, M.; Walter, A. Self-Diffusion of n-Paraffins in NaX Zeolite. J. Chem. Soc. Faraday Trans. 1 Phys. Chem. Condens. Phases 1980, 76 (0), 717. https://doi.org/10.1039/f19807600717.

(33) Siddiqui, M. A. Q.; Salvemini, F.; Ramandi, H. L.; Fitzgerald, P.; Roshan, H. Configurational Diffusion Transport of Water and Oil in Dual Continuum Shales. Sci. Rep. 2021, 11 (1), 2152. https://doi.org/10.1038/s41598-021-81004-1.

(34) Li, K.; Valla, J.; Garcia-Martinez, J. Realizing the Commercial Potential of Hierarchical Zeolites: New Opportunities in Catalytic Cracking. ChemCatChem 2014, 6 (1), 46–66. https://doi.org/10.1002/cctc.201300345.

(35) Shi, J.; Wang, Y.; Yang, W.; Tang, Y.; Xie, Z. Recent Advances of Pore System Construction in Zeolite-Catalyzed Chemical Industry Processes. Chem. Soc. Rev. 2015, 44 (24), 8877–8903. https://doi.org/10.1039/C5CS00626K.

(36) Mintova, S.; Gilson, J.-P.; Valtchev, V. Advances in Nanosized Zeolites. Nanoscale 2013, 5 (15), 6693. https://doi.org/10.1039/c3nr01629c.

(37) Feliczak-Guzik, A. Hierarchical Zeolites: Synthesis and Catalytic Properties. Microporous Mesoporous Mater. 2018, 259, 33–45. https://doi.org/10.1016/j.micromeso.2017.09.030.

(38) Christensen, C.; Johannsen, K.; Tornqvist, E.; Schmidt, I.; Topsoe, H.; Christensen, C. Mesoporous Zeolite Single Crystal Catalysts: Diffusion and Catalysis in Hierarchical Zeolites. Catal. Today 2007, 128 (3–4), 117–122. https://doi.org/10.1016/j.cattod.2007.06.082.

(39) Arstad, B.; Kolboe, S. The Reactivity of Molecules Trapped within the SAPO-34 Cavities in the Methanol-to-Hydrocarbons Reaction. J. Am. Chem. Soc. 2001, 123 (33), 8137–8138. https://doi.org/10.1021/ja010668t.

(40) Li, L.; Cui, X.; Li, J.; Wang, J. Synthesis of SAPO-34/ZSM-5 Composite and Its Catalytic Performance in the Conversion of Methanol to Hydrocarbonsc. J. Braz. Chem. Soc. 2014. https://doi.org/10.5935/0103-5053.20140279.

(41) Heering, J.; Kotter, M.; Reikert, L. Diffusion and Catalytic Reaction in Zeolite ZSM-5. Chem. Eng. Sci. 1982, 37 (4), 581–584. https://doi.org/10.1016/0009-2509(82)80120-6.

(42) Zhao, T.-S.; Takemoto, T.; Tsubaki, N. Direct Synthesis of Propylene and Light Olefins from Dimethyl Ether Catalyzed by Modified H-ZSM-5. Catal. Commun. 2006, 7 (9), 647–650. https://doi.org/10.1016/j.catcom.2005.11.009.

(43) Möller, K. P.; Kojima, M.; O'Connor, C. T. Diffusion and Adsorption in Zeolite Y and Mordenite Deactivated by Propene Oligomerization and Hexane Cracking. Chem. Eng. J. Biochem. Eng. J. 1994, 54 (3), 115–123. https://doi.org/10.1016/0923-0467(94)00203-7.

(44) Askari, S.; Halladj, R.; Sohrabi, M. Methanol Conversion to Light Olefins over Sonochemically Prepared SAPO-34 Nanocatalyst. Microporous Mesoporous Mater. 2012, 163, 334–342. https://doi.org/10.1016/j.micromeso.2012.07.041.

(45) Young, L. Shape Selective Reactions with Zeolite Catalysts III. Selectivity in Xylene Isomerization, Toluene-Methanol Alkylation, and Toluene Disproportionation over ZSM-5 Zeolite Catalysts. J. Catal. 1982, 76 (2), 418–432. https://doi.org/10.1016/0021-9517(82)90271-8.

(46) Catalytic Materials: Relationship Between Structure and Reactivity; Whyte, T. E., Dalla Betta, R. A., Derouane, E. G., Baker, R. T. K., Eds.; ACS Symposium Series; American Chemical Society: Washington, D.C., 1984; Vol. 248. https://doi.org/10.1021/bk-1984-0248.

(47) Voogd, P.; Van Bekkum, H. Limitation of N-Hexane and 3-Methylpentane Conversion over Zeolite ZSM-5 by Intracrystalline Diffusion. Appl. Catal. 1990, 59 (1), 311–331. https://doi.org/10.1016/S0166-9834(00)82206-X.

(48) Silaghi, M.-C.; Chizallet, C.; Raybaud, P. Challenges on Molecular Aspects of Dealumination and Desilication of Zeolites. Microporous Mesoporous Mater. 2014, 191, 82–96. https://doi.org/10.1016/j.micromeso.2014.02.040.

(49) Peng, P.; Gao, X.-H.; Yan, Z.-F.; Mintova, S. Diffusion and Catalyst Efficiency in Hierarchical Zeolite Catalysts. Natl. Sci. Rev. 2020, 7 (11), 1726–1742. https://doi.org/10.1093/nsr/nwaa184.

(50) Hartmann, M.; Thommes, M.; Schwieger, W. Hierarchically-Ordered Zeolites: A Critical Assessment. Adv. Mater. Interfaces 2021, 8 (4), 2001841. https://doi.org/10.1002/admi.202001841.

(51) Airi, A.; Signorile, M.; Bonino, F.; Quagliotto, P.; Bordiga, S.; Martens, J. A.; Crocellà, V. Insights on a Hierarchical MFI Zeolite: A Combined Spectroscopic and Catalytic Approach for Exploring the Multilevel Porous System Down to the Active Sites. ACS Appl. Mater. Interfaces 2021, 13 (41), 49114–49127. https://doi.org/10.1021/acsami.1c11614.

(52) Galarneau, A.; Guenneau, F.; Gedeon, A.; Mereib, D.; Rodriguez, J.; Fajula, F.; Coasne, B. Probing Interconnectivity in Hierarchical Microporous/Mesoporous Materials Using Adsorption and Nuclear Magnetic Resonance Diffusion. J. Phys. Chem. C 2016, 120 (3), 1562–1569. https://doi.org/10.1021/acs.jpcc.5b10129.

(53) Li, S.-C.; Lin, Y.-C.; Li, Y.-P. Understanding the Catalytic Activity of Microporous and Mesoporous Zeolites in Cracking by Experiments and Simulations. Catalysts 2021, 11 (9), 1114. https://doi.org/10.3390/catal11091114.

(54) Wang, X.; Zhang, J.; Zhang, T.; Xiao, H.; Song, F.; Han, Y.; Tan, Y. Mesoporous ZnZSM-5 Zeolites Synthesized by One-Step Desilication and Reassembly: A Durable Catalyst for Methanol Aromatization. RSC Adv. 2016, 6 (28), 23428–23437. https://doi.org/10.1039/C6RA03511F.

(55) Bonilla, M. R.; Valiullin, R.; Kärger, J.; Bhatia, S. K. Understanding Adsorption and Transport of Light Gases in Hierarchical Materials Using Molecular Simulation and Effective Medium Theory. J. Phys. Chem. C 2014, 118 (26), 14355–14370. https://doi.org/10.1021/jp5028228.

(56) Gorring, R. Diffusion of Normal Paraffins in Zeolite T Occurrence of Window Effect. J. Catal. 1973, 31 (1), 13–26. https://doi.org/10.1016/0021-9517(73)90265-0.

(57) Yucel, H.; Ruthven, D. M. Diffusion of CO2 in 4A and 5A Zeolite Crystals. J. Colloid Interface Sci. 1980, 74 (1), 186–195. https://doi.org/10.1016/0021-9797(80)90182-4.

(58) Zhai, D.; Zhao, L.; Gao, J.; Xu, C. Effect of Temperature on the Diffusion Mechanism of Xylene Isomers in a FAU Zeolite: A Molecular Dynamics Study. Phys. Chem. Chem. Phys. 2012, 14 (20), 7296. https://doi.org/10.1039/c2cp40584a.

(59) Wang, S.; Zhang, Y.; Wu, H.; Lee, S. H.; Qiao, R.; Wen, X.-H. A Kinetic Model for Multicomponent Gas Transport in Shale Gas Reservoirs and Its Applications. Phys. Fluids 2022, 34 (8), 082002. https://doi.org/10.1063/5.0101272.

(60) Sazhin, S. S.; Shishkova, I. N.; Kryukov, A. P.; Levashov, V. Yu.; Heikal, M. R. Evaporation of Droplets into a Background Gas: Kinetic Modelling. Int. J. Heat Mass Transf. 2007, 50 (13–14), 2675–2691. https://doi.org/10.1016/j.ijheatmasstransfer.2006.11.043.

(61) Xu, K.; Martinelli, L.; Jameson, A. Gas-Kinetic Finite Volume Methods, Flux-Vector Splitting, and Artificial Diffusion. J. Comput. Phys. 1995, 120 (1), 48–65. https://doi.org/10.1006/jcph.1995.1148.

(62) Chandrasekhar, S. Stochastic Problems in Physics and Astronomy. Rev. Mod. Phys. 1943, 15 (1), 1–89. https://doi.org/10.1103/RevModPhys.15.1.

(63) Einstein, A. Über die von der molekularkinetischen Theorie der Wärme geforderte Bewegung von in ruhenden Flüssigkeiten suspendierten Teilchen. Ann. Phys. 1905, 322 (8), 549–560. https://doi.org/10.1002/andp.19053220806.

(64) Sutherland, W. LXXV. A Dynamical Theory of Diffusion for Non-Electrolytes and the Molecular Mass of Albumin. Lond. Edinb. Dublin Philos. Mag. J. Sci. 1905, 9 (54), 781–785. https://doi.org/10.1080/14786440509463331.

(65) Schoberth, S. M.; Bär, N.-K.; Krämer, R.; Kärger, J. Pulsed High-Field Gradient in Vivo NMR Spectroscopy to Measure Diffusional Water Permeability in Corynebacterium Glutamicum. Anal. Biochem. 2000, 279 (1), 100–105. https://doi.org/10.1006/abio.1999.4450.

(66) Gusev, A. A.; Suter, U. W.; Moll, D. J. Relationship between Helium Transport and Molecular Motions in a Glassy Polycarbonate. Macromolecules 1995, 28 (7), 2582–2584. https://doi.org/10.1021/ma00111a065.

(67) Andre, J. C.; Baros, F.; Sousa, A. T. R. E. Kinetics of Partly Diffusion-Controlled Reaction XXI: A Simple Algorithm for Computing the Apparent Rate of Reaction. Int. J. Chem. Kinet. 1989, 21 (5), 297–314. https://doi.org/10.1002/kin.550210502.

(68) Das, A. K. Note on Stochastic Dynamics in a Coulomb Field. Chem. Phys. 1981, 54 (2), 249–252. https://doi.org/10.1016/0301-0104(81)80239-X.

(69) Comyn, J. Introduction to Polymer Permeability and the Mathematics of Diffusion. In Polymer Permeability; Comyn, J., Ed.; Springer Netherlands: Dordrecht, 1985; pp 1–10. https://doi.org/10.1007/978-94-009-4858-7_1.

(70) Erdelyi, Z. On the ?Rationalisation? Of Fick?S First Law. Scr. Mater. 2003, 49 (6), 613–617. https://doi.org/10.1016/S1359-6462(03)00353-1.

(71) Rehage, G.; Ernst, O.; Fuhrmann, J. Fickian and Non-Fickian Diffusion in High Polymer Systems. Discuss. Faraday Soc. 1970, 49, 208. https://doi.org/10.1039/df9704900208.

(72) Ferreira, J. A.; Grassi, M.; Gudiño, E.; de Oliveira, P. A New Look to Non-Fickian Diffusion. Appl. Math. Model. 2015, 39 (1), 194–204. https://doi.org/10.1016/j.apm.2014.05.030.

(73) De Kee, D.; Liu, Q.; Hinestroza, J. Viscoelastic (Non-Fickian) Diffusion. Can. J. Chem. Eng. 2008, 83 (6), 913–929. https://doi.org/10.1002/cjce.5450830601.

(74) Malek, K.; Coppens, M.-O. Effects of Surface Roughness on Self- and Transport Diffusion in Porous Media in the Knudsen Regime. Phys. Rev. Lett. 2001, 87 (12), 125505. https://doi.org/10.1103/PhysRevLett.87.125505.

(75) Tsuru, T.; Takata, Y.; Kondo, H.; Hirano, F.; Yoshioka, T.; Asaeda, M. Characterization of Sol–Gel Derived Membranes and Zeolite Membranes by Nanopermporometry. Sep. Purif. Technol. 2003, 32 (1–3), 23–27. https://doi.org/10.1016/S1383-5866(03)00036-4.

(76) Shariati, V.; Ahmadian, M. H.; Roohi, E. Direct Simulation Monte Carlo Investigation of Fluid Characteristics and Gas Transport in Porous Microchannels. Sci. Rep. 2019, 9 (1), 17183. https://doi.org/10.1038/s41598-019-52707-3.

(77) Levitz, P. Knudsen Diffusion and Excitation Transfer in Random Porous Media. J. Phys. Chem. 1993, 97 (15), 3813–3818. https://doi.org/10.1021/j100117a030.

(78) Kunze, S.; Groll, R.; Besser, B.; Thöming, J. Molecular Diameters of Rarefied Gases. Sci. Rep. 2022, 12 (1), 2057. https://doi.org/10.1038/s41598-022-05871-y.

(79) Liu, J.; Wei, J. Knudsen Diffusion in Channels and Networks. Chem. Eng. Sci. 2014, 111, 1–14. https://doi.org/10.1016/j.ces.2014.01.014.

(80) Coulson, C. A. The Mathematics of Diffusion. By J. Crank. Pp. Vii, 347. 50s. 1956. (Clarendon Press). Math. Gaz. 1958, 42 (340), 165–165. https://doi.org/10.2307/3609455.

(81) Lynch, J. C.; Brannon, J. M.; Hatfield, K.; Delfino, J. J. An Exploratory Approach to Modeling Explosive Compound Persistence and Flux Using Dissolution Kinetics. J. Contam. Hydrol. 2003, 66 (3–4), 147–159. https://doi.org/10.1016/S0169-7722(03)00030-5.

(82) Hall, L. D. Nuclear Magnetic Resonance. In Advances in Carbohydrate Chemistry; Elsevier, 1964; Vol. 19, pp 51–93. https://doi.org/10.1016/S0096-5332(08)60279-9.

(83) Barth, B. A.; Imel, A.; Nelms, K. M.; Goenaga, G. A.; Zawodzinski, T. Microemulsions: Breakthrough Electrolytes for Redox Flow Batteries. Front. Chem. 2022, 10, 831200. https://doi.org/10.3389/fchem.2022.831200.

(84) Valfouskaya, A.; Adler, P. M.; Thovert, J.-F.; Fleury, M. Nuclear-Magnetic-Resonance Diffusion Simulations in Porous Media. J. Appl. Phys. 2005, 97 (8), 083510. https://doi.org/10.1063/1.1871352.

(85) Kärger, J.; Pfeifer, H. N.m.r. Self-Diffusion Studies in Zeolite Science and Technology. Zeolites 1987, 7 (2), 90–107. https://doi.org/10.1016/0144-2449(87)90067-4.

(86) Kärger, J. NMR Self-Diffusion Studies in Heterogeneous Systems. Adv. Colloid Interface Sci. 1985, 23, 129–148. https://doi.org/10.1016/0001-8686(85)80018-X.

(87) Crutchfield, C. A.; Harris, D. J. Molecular Mass Estimation by PFG NMR Spectroscopy. J. Magn. Reson. 2007, 185 (1), 179–182. https://doi.org/10.1016/j.jmr.2006.12.004.

(88) Topgaard, D.; Söderman, O. Experimental Determination of Pore Shape and Size Using Q-Space NMR Microscopy in the Long Diffusion-Time Limit. Magn. Reson. Imaging 2003, 21 (1), 69–76. https://doi.org/10.1016/S0730-725X(02)00626-4.

(89) Valfouskaya, A.; Adler, P. M.; Thovert, J.-F.; Fleury, M. Nuclear Magnetic Resonance Diffusion with Surface Relaxation in Porous Media. J. Colloid Interface Sci. 2006, 295 (1), 188–201. https://doi.org/10.1016/j.jcis.2005.08.021.

(90) Malik, M. I.; Pasch, H. Basic Principles of Size Exclusion and Liquid Interaction Chromatography of Polymers. In Molecular Characterization of Polymers; Elsevier, 2021; pp 1–59. https://doi.org/10.1016/B978-0-12-819768-4.00007-5.

(91) Franconi, F.; Lemaire, L.; Gimel, J.-C.; Bonnet, S.; Saulnier, P. NMR Diffusometry: A New Perspective for Nanomedicine Exploration. J. Controlled Release 2021, 337, 155–167. https://doi.org/10.1016/j.jconrel.2021.07.025.

(92) Falcioni, M.; Deem, M. W. A Biased Monte Carlo Scheme for Zeolite Structure Solution. J. Chem. Phys. 1999, 110 (3), 1754–1766. https://doi.org/10.1063/1.477812.

(93) Hahn, E. L. Spin Echoes. Phys. Rev. 1950, 80 (4), 580–594. https://doi.org/10.1103/PhysRev.80.580.

(94) Stejskal, E. O.; Tanner, J. E. Spin Diffusion Measurements: Spin Echoes in the Presence of a Time-Dependent Field Gradient. J. Chem. Phys. 1965, 42 (1), 288–292. https://doi.org/10.1063/1.1695690.

(95) Tanner, J. E. Use of the Stimulated Echo in NMR Diffusion Studies. J. Chem. Phys. 1970, 52 (5), 2523–2526. https://doi.org/10.1063/1.1673336.

(96) Tanner, J. E. Pulsed Field Gradients for NMR Spin-Echo Diffusion Measurements. Rev. Sci. Instrum. 1965, 36 (8), 1086–1087. https://doi.org/10.1063/1.1719808.

(97) Tanner, J. E.; Stejskal, E. O. Restricted Self-Diffusion of Protons in Colloidal Systems by the Pulsed-Gradient, Spin-Echo Method. J. Chem. Phys. 1968, 49 (4), 1768–1777. https://doi.org/10.1063/1.1670306.

(98) Kuchel, P. W.; Pagès, G.; Nagashima, K.; Velan, S.; Vijayaragavan, V.; Nagarajan, V.; Chuang, K. H. Stejskal-Tanner Equation Derived in Full. Concepts Magn. Reson. Part A 2012, 40A (5), 205–214. https://doi.org/10.1002/cmr.a.21241.

(99) Woessner, D. E. N.M.R. SPIN-ECHO SELF-DIFFUSION MEASUREMENTS ON FLUIDS UNDERGOING RESTRICTED DIFFUSION. J. Phys. Chem. 1963, 67 (6), 1365–1367. https://doi.org/10.1021/j100800a509.

(100) Kärger, J.; Ruthven, D. M. Diffusion in Nanoporous Materials: Fundamental Principles, Insights and Challenges. New J. Chem. 2016, 40 (5), 4027–4048. https://doi.org/10.1039/C5NJ02836A.

(101) Kortunov, P.; Vasenkov, S.; Chmelik, C.; Kärger, J.; Ruthven, D. M.; Wloch, J. Influence of Defects on the External Crystal Surface on Molecular Uptake into MFI-Type Zeolites. Chem. Mater. 2004, 16 (18), 3552–3558. https://doi.org/10.1021/cm0401645.

(102) Titze, T.; Lauerer, A.; Heinke, L.; Chmelik, C.; Zimmermann, N. E. R.; Keil, F. J.; Ruthven, D. M.; Kärger, J. Transport in Nanoporous Materials Including MOFs: The Applicability of Fick's Laws. Angew. Chem. Int. Ed. 2015, 54 (48), 14580–14583. https://doi.org/10.1002/anie.201506954.

(103) Jobic, H.; Kärger, J.; Krause, C.; Brandani, S.; Gunadi, A.; Methivier, A.; Ehlers, G.; Farago, B.; Haeussler, W.; Ruthven, D. M. Diffusivities of N-Alkanes in 5A Zeolite Measured by Neutron Spin Echo, Pulsed-Field Gradient NMR, and Zero Length Column Techniques. Adsorption 2005, 11 (S1), 403–407. https://doi.org/10.1007/s10450-005-5958-8.

(104) Banas, K.; Brandani, F.; Ruthven, D. M.; Stallmach, F.; Kärger, J. Combining Macroscopic and Microscopic Diffusion Studies in Zeolites Using NMR Techniques. Magn. Reson. Imaging 2005, 23 (2), 227–232. https://doi.org/10.1016/j.mri.2004.11.015.

(105) Kalachandra, S.; Turner, D. T. Water Sorption of Polymethacrylate Networks: Bis-GMA/TEGDM Copolymers. J. Biomed. Mater. Res. 1987, 21 (3), 329–338. https://doi.org/10.1002/jbm.820210306.

(106) Barrer, R. M.; Rees, L. V. C. Self-Diffusion of Alkali Metal Ions in Analcite. Trans. Faraday Soc. 1960, 56, 709. https://doi.org/10.1039/tf9605600709.

(107) Hong, U.; Kärger, J.; Kramer, R.; Pfeifer, H.; Seiffert, G.; Müller, U.; Unger, K. K.; Lück, H.-B.; Ito, T. PFG n.m.r. Study of Diffusion Anisotropy in Oriented ZSM-5 Type Zeolite Crystallites. Zeolites 1991, 11 (8), 816–821. https://doi.org/10.1016/S0144-2449(05)80061-2.

(108) Grenier; Meunier, F.; Gray, P. G.; Kärger, J.; Xu, Z.; Ruthven, D. M. Diffusion of Methanol in NaX Crystals: Comparison of i.r., ZLC, and PFG-n.m.r. Measurements. Zeolites 1994, 14 (4), 242–249. https://doi.org/10.1016/0144-2449(94)90091-4.

(109) Price, W. S.; Ide, H.; Arata, Y. Self-Diffusion of Supercooled Water to 238 K Using PGSE NMR Diffusion Measurements. J. Phys. Chem. A 1999, 103 (4), 448–450. https://doi.org/10.1021/jp9839044.

(110) Price, W. S.; Tsuchiya, F.; Arata, Y. Lysozyme Aggregation and Solution Properties Studied Using PGSE NMR Diffusion Measurements. J. Am. Chem. Soc. 1999, 121 (49), 11503–11512. https://doi.org/10.1021/ja992265n.

(111) Chmelik, C.; Freude, D.; Bux, H.; Haase, J. Ethene/Ethane Mixture Diffusion in the MOF Sieve ZIF-8 Studied by MAS PFG NMR Diffusometry. Microporous Mesoporous Mater. 2012, 147 (1), 135–141. https://doi.org/10.1016/j.micromeso.2011.06.009.

(112) Wehring, M.; Gascon, J.; Dubbeldam, D.; Kapteijn, F.; Snurr, R. Q.; Stallmach, F. Self-Diffusion Studies in CuBTC by PFG NMR and MD Simulations. J. Phys. Chem. C 2010, 114 (23), 10527–10534. https://doi.org/10.1021/jp102212w.

(113) Bachus, R.; Kimmich, R. Molecular Weight and Temperature Dependence of Self-Diffusion Coefficients in Polyethylene and Polystyrene Melts Investigated Using a Modified n.m.r. Field-Gradient Technique. Polymer 1983, 24 (8), 964–970. https://doi.org/10.1016/0032-3861(83)90146-5.

(114) Hemelsoet, K.; Ghysels, A.; Mores, D.; De Wispelaere, K.; Van Speybroeck, V.; Weckhuysen, B. M.; Waroquier, M. Experimental and Theoretical IR Study of Methanol and Ethanol Conversion over H-SAPO-34. Catal. Today 2011, 177 (1), 12–24. https://doi.org/10.1016/j.cattod.2011.05.040.

(115) Berens, S.; Chmelik, C.; Hillman, F.; Kärger, J.; Jeong, H.-K.; Vasenkov, S. Ethane Diffusion in Mixed Linker Zeolitic Imidazolate Framework-7-8 by Pulsed Field Gradient NMR in Combination with Single Crystal IR Microscopy. Phys. Chem. Chem. Phys. 2018, 20 (37), 23967–23975. https://doi.org/10.1039/C8CP04889D.

(116) Mueller, R.; Hariharan, V.; Zhang, C.; Lively, R.; Vasenkov, S. Relationship between Mixed and Pure Gas Self-Diffusion for Ethane and Ethene in ZIF-8/6FDA-DAM Mixed-Matrix Membrane by Pulsed Field Gradient NMR. J. Membr. Sci. 2016, 499, 12–19. https://doi.org/10.1016/j.memsci.2015.10.036.

(117) Wouters, B. H.; Chen, T.; Grobet, P. J. Steaming of Zeolite Y: Formation of Transient Al Species. J. Phys. Chem. B 2001, 105 (6), 1135–1139. https://doi.org/10.1021/jp001620p.

(118) Zhang, L.; Chen, K.; Chen, B.; White, J. L.; Resasco, D. E. Factors That Determine Zeolite Stability in Hot Liquid Water. J. Am. Chem. Soc. 2015, 137 (36), 11810–11819. https://doi.org/10.1021/jacs.5b07398.

(119) Pfeiffer, W. T.; Bauer, S. Subsurface Porous Media Hydrogen Storage – Scenario Development and Simulation. Energy Procedia 2015, 76, 565–572. https://doi.org/10.1016/j.egypro.2015.07.872.

(120) Erfani, A.; Szutkowski, K.; Aichele, C. P.; White, J. L. Diffusion, Interactions, and Disparate Kinetic Trapping of Water–Hydrocarbon Mixtures in Nanoporous Solids. Langmuir 2021, 37 (2), 858–866. https://doi.org/10.1021/acs.langmuir.0c03201.

(121) Ardelean, I.; Mattea, C.; Farrher, G.; Wonorahardjo, S.; Kimmich, R. Nuclear Magnetic Resonance Study of the Vapor Phase Contribution to Diffusion in Nanoporous Glasses Partially Filled with Water and Cyclohexane. J. Chem. Phys. 2003, 119 (19), 10358–10362. https://doi.org/10.1063/1.1618214.

(122) Cammack, R. EPR, Methods. In Encyclopedia of Spectroscopy and Spectrometry; Elsevier, 2017; pp 527–538. https://doi.org/10.1016/B978-0-12-803224-4.00138-2.

(123) Holz, M.; Heil, S. R.; Sacco, A. Temperature-Dependent Self-Diffusion Coefficients of Water and Six Selected Molecular Liquids for Calibration in Accurate 1H NMR PFG Measurements. Phys. Chem. Chem. Phys. 2000, 2 (20), 4740–4742. https://doi.org/10.1039/b005319h.

(124) Lee, D. K.; In, J.; Lee, S. Standard Deviation and Standard Error of the Mean. Korean J. Anesthesiol. 2015, 68 (3), 220. https://doi.org/10.4097/kjae.2015.68.3.220.

(125) Abdolrahmani, M.; Chen, K.; White, J. L. Assessment, Control, and Impact of Brønsted Acid Site Heterogeneity in Zeolite HZSM-5. J. Phys. Chem. C 2018, 122 (27), 15520–15528. https://doi.org/10.1021/acs.jpcc.8b04283.

(126) Maghsoudi, H.; Nozari, V.; Zamzami, S. R. Diffusion of Methane in High-Silica CHA Zeolite. Heat Mass Transf. 2019, 55 (6), 1619–1625. https://doi.org/10.1007/s00231-018-02547-0.

(127) Berens, S.; Hillman, F.; Jeong, H.-K.; Vasenkov, S. Self-Diffusion of Pure and Mixed Gases in Mixed-Linker Zeolitic Imidazolate Framework-7-8 by High Field Diffusion NMR. Microporous Mesoporous Mater. 2019, 288, 109603. https://doi.org/10.1016/j.micromeso.2019.109603.

(128) Baniani, A.; Chmelik, C.; Forman, E. M.; Fan, L.; Zhou, E.; Zhang, F.; Lyndon, R.; Lively, R. P.; Vasenkov, S. Anomalous Relationship between Molecular Size and Diffusivity of Ethane and Ethylene inside Crystals of Zeolitic Imidazolate Framework-11. J. Phys. Chem. C 2019, 123 (27), 16813–16822. https://doi.org/10.1021/acs.jpcc.9b03933.

(129) Chen, K.; Zornes, A.; Bababrik, R.; Crouch, J.; Alvarez, W.; Wulfers, M.; Resasco, D.; Wang, B.; Crossley, S.; White, J. L. First-Formed Framework Species and Phosphate Structure Distributions in Phosphorus-Modified MFI Zeolites. J. Phys. Chem. C 2022, 126 (1), 227–238. https://doi.org/10.1021/acs.jpcc.1c08448.

(130) Lee, E. F. T.; Rees, L. V. C. Effect of Calcination on Location and Valency of Lanthanum Ions in Zeolite Y. Zeolites 1987, 7 (2), 143–147. https://doi.org/10.1016/0144-2449(87)90076-5.

(131) Vu, H.-T.; Goepel, M.; Gläser, R. Improving the Hydrothermal Stability of Zeolite Y by La 3+ Cation Exchange as a Catalyst for the Aqueous-Phase Hydrogenation of Levulinic Acid. RSC Adv. 2021, 11 (10), 5568–5579. https://doi.org/10.1039/D0RA08907A.

(132) Gil, A.; Vicente, M. A. Energy Storage Materials from Clay Minerals and Zeolite-like Structures. In Modified Clay and Zeolite Nanocomposite Materials; Elsevier, 2019; pp 275–288. https://doi.org/10.1016/B978-0-12-814617-0.00005-0.

(133) Langmi, H. W.; Book, D.; Walton, A.; Johnson, S. R.; Al-Mamouri, M. M.; Speight, J. D.; Edwards, P. P.; Harris, I. R.; Anderson, P. A. Hydrogen Storage in Ion-Exchanged Zeolites. J. Alloys Compd. 2005, 404–406, 637–642. https://doi.org/10.1016/j.jallcom.2004.12.193.

(134) Li, Y.; Yang, R. T. Hydrogen Storage in Low Silica Type X Zeolites. J. Phys. Chem. B 2006, 110 (34), 17175–17181. https://doi.org/10.1021/jp0634508.

(135) Ge, L.; Qiu, M.; Zhu, Y.; Yang, S.; Li, W.; Li, W.; Jiang, Z.; Chen, X. Synergistic Catalysis of Ru Single-Atoms and Zeolite Boosts High-Efficiency Hydrogen Storage. Appl. Catal. B Environ. 2022, 319, 121958. https://doi.org/10.1016/j.apcatb.2022.121958.

(136) Cavenati, S.; Grande, C. A.; Rodrigues, A. E. Removal of Carbon Dioxide from Natural Gas by Vacuum Pressure Swing Adsorption. Energy Fuels 2006, 20 (6), 2648–2659. https://doi.org/10.1021/ef060119e.

APPENDICES

.

a.

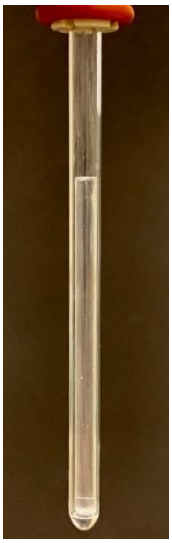

b.

c.

Figure 21. a. NPG in NMR tube b. NPG c. Zeolites in NMR tube beside a measuring scale.

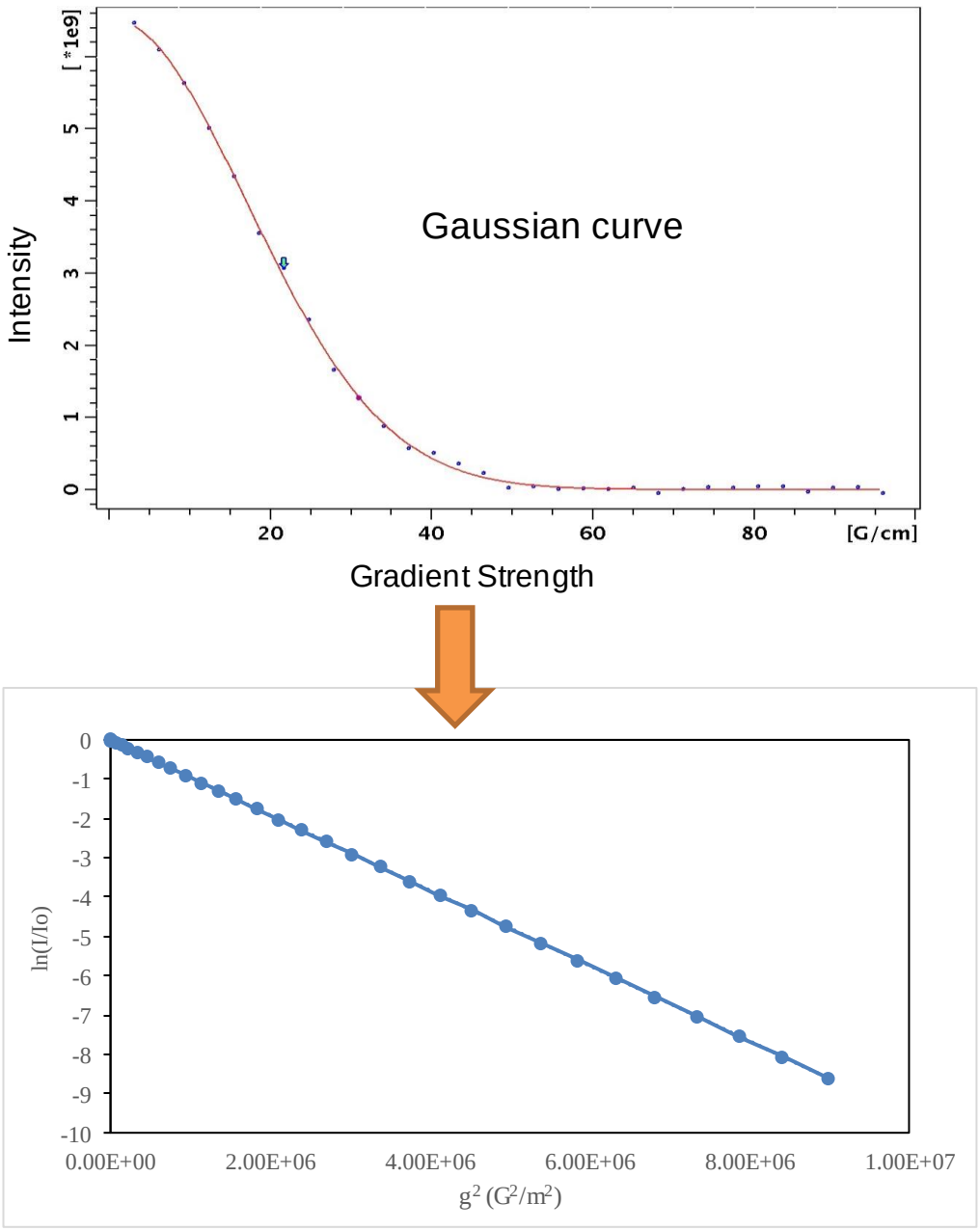

Figure 22. NMR data processing

Figure 23. NMR Bruker 400 MHz (9.4 T) NMR spectrometer

Figure 24. Diffusion probe, gradient strengths up to 2900 Gauss/cm

VITA

Moumita Biswas

Candidate for the Degree of

Master of Science

Thesis: DIFFUSION OF GASES AND LIQUIDS IN NANOPOROUS SOLIDS

Major Field: Chemical Engineering

Biographical:

Education:

Completed the requirements for the Master of Science in Chemical Engineering at Oklahoma State University, Stillwater, Oklahoma in May, 2023.

Completed the requirements for the Master of Business Administration at Indian Institute of Technology in 2018.

Completed the requirements for the Bachelor of Technology in Chemical Engineering at West Bengal University of Technology in 2016.

Experience:

Sales Associate at Nettare Beverages Private Limited from September, 2018 till January, 2019.

Summer Intern at Berger Paints India from June, 2015 till July, 2015.

Certification:

Completed Lean Six Sigma Certification, Green Belt, offered by KPMG in April, 2017.

Completed the certification, An Introduction to Interactive Programming in Python, offered by Rice University, in July, 2022.